Fall 11-2020

Effect of Cold Work Expansion on the Fatigue Life of Pre-Cracked Al 2024-T3

Christopher Leirer
Embry-Riddle Aeronautical University

EFFECT OF COLD WORK EXPANSION ON THE FATIGUE LIFE OF PRE-CRACKED Al 2024-T3

By

Christopher Leirer

A Thesis Submitted to the Faculty of Embry-Riddle Aeronautical University

In Partial Fulfillment of the Requirements for the Degree of

Master of Science in Aerospace Engineering

November 2020

Embry-Riddle Aeronautical University

Daytona Beach, Florida

EFFECT OF COLD WORK EXPANSION ON
THE FATIGUE LIFE OF PRE-CRACKED Al 2024-T3

By

Christopher Leirer

This Thesis was prepared under the direction of the candidate's Thesis Committee Chair, Dr. Alberto W. Mello, Department of Aerospace Engineering, and has been approved by the members of the Thesis Committee. It was submitted to the Office of the Senior Vice President for Academic Affairs and Provost, and was accepted in the partial fulfillment of the requirements for the Degree of Master of Science in Aerospace Engineering.

THESIS COMMITTEE

Chairman, Dr. Alberto W. Mello	Member, Dr. Daewon Kim
Member, Dr. David J. Sypeck	
Graduate Program Coordinator, Dr. Marwan Al-Haik	Date
Dean of the College of Engineering, Dr. Maj Mirmirani	Date
Associate Provost of Academic Support, Dr. Christopher Grant	Date

ACKNOWLEDGEMENTS

The work of this thesis would not be possible without the following people. Firstly, I would like to thank my committee chair, Dr. Alberto W. Mello, thank you so much for providing instruction and guidance throughout this process. You made the difficult topics come off as simple and I could not have done it without you. I would also like to thank my committee members, Dr. Daewon Kim and Dr. David J. Sypeck, you both challenged me and compelled me to think outside the box to better my research.

I would like to thank my friend and research partner, Ken Shishino, you went through a lot of this with me from the highs to the lows both academically and personally, and for that, I am incredibly grateful for all that you have done for me throughout the years. To my roommates, Zachary Bryant, Kody Miller, Parker Tyson, and Chase Williams, thank you for all the emotional and mental support throughout my whole college career. Without the late, sometimes too late, nights I do not know how I would be able to make it through all this while being still sane.

I would like to thank my family, Dad, my sister Alex, and my two grandmothers, thank you for always believing in me even though I did not believe in myself, I love you all. To Dr. Pamela Daniels, you took me in when I needed it most and have always been there to provide emotional support or a swift kick in the rear to get me going, I truly view you as a second mother and I am so glad to have you. Lastly, and certainly not least, I would like to thank my mother. You are my beautiful angel in heaven looking out for me and if it was not for you I never would have accomplished all that I have in these five and a half years, I hope that I have made you proud and know that I strive to continue to do that. “I love you to the moon and back times infinity squared, Momma!”

ABSTRACT

The manufacturing and preparation of alloys normally include processes to improve their resistance to crack growth and fatigue endurance for structural application. The benefits of cold expansion are well known, and its application is widely used in new and repaired structures, even in crack arrester holes. When applied in the field, damaged material removal in a cold expansion procedure may be limited to a maximum allowable diameter for reaming and finishing, which may leave small cracks on the strained region. To completely understand the effect of initial cracks as a function of initial plastic deformation level in a cold-worked hole it is necessary to fully evaluate stress/strain distribution during and post cold expansion.

For the completion of this thesis, Al 2024-T3 samples were dimensioned and manufactured following best practices and results from classic plasticity theories. Analytical stress and strain calculations were compared to numerical solutions from elastic-plastic analysis using NX Nastran FEMAP, as well as experimental strain measurements calculated by calibrated Digital Image Correlation with the use of images taken during the cold-working process. The fatigue life was compared between pre-cracked open and cold expanded specimens. The crack growth was monitored using a digital optical microscope. The full analysis and stress/strain maps can help in further development to simulate a typical aerospace application, with test of a cold-worked hole in presence of a galvanic couple under aggressive environment to establish the impact of local residual stress in crack growth acceleration or formation of new cracks.

TABLE OF CONTENTS

LIST OF FIGURES

Figure Page

Figure Page

Figure Page

LIST OF TABLES

SYMBOLS

a	Radius of fastener hole
b	Half of system external diameter
c	Radius of plastic zone
D_{in}	Fastener hole diameter
D_m	Mandrel diameter
E	Young's Modulus of Elasticity
G	Shear Modulus
P_c	Internal pressure to cause yielding to plastic zone radius
P_{y_i}	Pressure required to yield material due to shear stress
P_{y_f}	Pressure required to cause full yielding of plastic region
R	Stress ratio
r	Distance from edge of hole
r_y	Reverse yielding radius
t_s	Sleeve thickness
U_{in}	Inward radial displacement
U_m	Radial displacement produced by mandrel
ε_2	Axial strain
ν	Poison ratio
σ_a	Amplitude stress
$\sigma_{r_{el}}$	Radial residual stress in elastic region
$\sigma_{t_{el}}$	Tangential residual stress in elastic region
σ_m	Average (mean) stress

σ_{max}	Maximum stress
σ_{min}	Minimum stress
$\sigma_{r_{pl}}$	Radial residual stress in plastic region
$\sigma_{t_{pl}}$	Tangential residual stress in plastic region
σ_r	Radial residual stress
$\sigma_{r_{ry}}$	Radial residual stress in reverse yielding region
$\sigma_{t_{ry}}$	Tangential residual stress in reverse yielding region
σ_t	Tangential residual stress
σ_y	Yield stress
σ_{yy}^{res}	Maximum residual stress
τ_y	Yield shear stress

ABBREVIATIONS

CE	Cold expansion
DIC	Digital Image Correlation
FEM	Finite Element Modeling
FTI	Fatigue Technology Incorporated
LSP	Laser Shock Peening
SEM	Scanning Electron Microscope

1. Introduction

The aerospace industry, like many industries, is highly cost-driven. The desire to decrease the cost of aircraft and aircraft service is something that dominates both the commercial aircraft field as well as in the military field. However, decreasing the cost of servicing aircraft without proper substantiation most often leads to cutting important corners, which may jeopardize safety and be the cause of catastrophic failures.

The servicing of aircraft can be for multiple reasons but the chief among them is fatigue of the aircraft, which will be discussed in detail later in this chapter. Fatigue can develop cracks in a structure that can yield to total structural failure of the material. Because of this, there has been a major investment from both an economic standpoint as well as a research aspect, in order to understand the phenomenon of fatigue and crack propagation. One research aspect is the ability to counter the effects of fatigue, which has resulted in many technologies to toughen the material and subsequently increase its strength and fatigue performance for standard aerospace applications. The aspects of material hardening used to create compressive residual stresses, the available technology to accomplish this task, and the materials and methods used in this research, such as cold expansion, will be discussed in subsequent sections of this chapter.

1.1. Overview of Fatigue

Failure of a structure is the process in which that structure can no longer support the loads and stresses that it was designed for. While structural failure is normally associated with a display of large destruction, it oftentimes begins on the smallest of scales at stress concentration regions. Stress concentrations, as the name implies, are regions of a structure or component that undergoes a higher amount of stress than other areas. Stress raisers are present in most type of structure, simply by the necessity of attachment holes

or eventually presence of sharp edges. However, geometric discontinuities may not be adequately predicted in the structural design phase, and the development of stress concentrations can occur for several reasons. Findlay and Harrison (2002) revealed through research that three of these unpredicted reasons as being: design errors, voids in the microstructure of the material, and corrosive attacks. The scope of this thesis will focus on geometric factors, either predicted or due to design error.

Design errors are often defined as discontinuities in the material, such as tight corners, notches, tight fillet radii, and the unpredicted presence of holes (Findlay & Harrison, 2002). While many of these design errors can be avoided, the presence of holes is largely unavoidable, mainly because of the way to attach components, such as wing-to-fuselage, skin/web-to-stringers, landing gear-to-fuselage/wing, etc. All joined together using fasteners such as bolts and rivets which require drilled holes. The process of drilling the hole may alter the level of stress concentration, due to imperfections that may be left at the hole border. During the drilling process there exist an increase in friction between the drill bit, the chips of metal that are being removed from the material, and the actual component being drilled, that introduces surface roughness on the hole wall which is what alters the level of the stress concentration (Sun et al., 2018).

An examination of records and accident cases was conducted by Findlay and Harrison (2002) and tabulated the frequencies of failure modes in aircraft. Their tabulation recreated in Table 1.1 shows that fatigue was found in 25% of the cases for general engineering components, and in 55% of aircraft components. When associated with other failure mechanisms, such as corrosion, this number will be higher than 60%. In addition to the investigation conducted by Findlay and Harrison (2002), another statistical analysis

shows that “fatigue fracture of fastener holes account for 50-90% of fracture of aging planes” (Liu et al., 2007, p. 35).

Table 1.1

Frequency of failure mechanisms in aircraft.

Percentage of Failures		
Failure Category	**Engineering Components**	**Aircraft Components**
Corrosion	29	16
Fatigue	25	55
Brittle fracture	16	-
Overload	11	14
High temperature corrosion	7	2
SCC/Corrosion fatigue/HE	6	7
Creep	3	-
Wear/abrasion/erosion	3	6

(Findlay & Harrison, 2002)

From the point of view of aircraft structural integrity programs, fatigue is the failure of an aircraft component that occurs because of cyclic loading. The failure most often occurs at a local stress value that is significantly below the component material yield stress, σ_y.

The fatigue performance of a component usually depends on a few parameters in relation to the loading environment that it is subjected to. The first control variable used to predict the fatigue performance is the experienced average stress, σ_m, which is the mean point between the minimum and maximum stress in a cycle. A higher mean stress for the same cyclic amplitude yields higher maximum stress and vice versa. The second variable that is normally used to predict the fatigue effect is the amplitude stress, σ_a,

which is determined based on the stress range within a cycle. The stress ratio, *R*, is another parameter that can be used as a control variable to determine fatigue performance and is the ratio between the minimum stress and maximum stress experienced in a cycle (Bandyopadhyay et al., 2019). A low-stress ratio is associated with high-stress amplitude. One important parameter for a fatigue test is the cycle frequency, which represents how many cycles the component experiences in a period of time. The former three variables can be seen represented in equation form in Equations 1 through 3, where, σ_{max}, is the maximum stress and, σ_{min}, is the minimum stress.

$$\sigma_m = \frac{\sigma_{max} + \sigma_{min}}{2} \tag{1}$$

$$\sigma_a = \frac{\sigma_{max} - \sigma_{min}}{2} \tag{2}$$

$$R = \frac{\sigma_{min}}{\sigma_{max}} \tag{3}$$

The repeated loading and then unloading begins to take a toll on the component eventually nucleating, initiating, and finally growing a crack (Dowling, 2012) which when grown to its critical length leads to complete failure. The nucleation and initiation of the crack more than likely will occur at the stress concentration regions as discussed before because the higher concentration of stresses combined with the cyclic loading conditions provide the localized high strains, which will eventually nucleate and initiate a crack (Nicolas et al., 2019). The propagation of the crack is caused by high stress experienced in the vicinity of the crack tip during the cyclic loading, which opens and closes the crack. This process is normally accelerated until it has reached its critical crack

length. At this critical crack length, the remaining material of the component is unable to support the nominal loading and complete failure occurs.

The initiation of the fatigue crack and the complete failure of the material has been the focus of many research projects as well as the development of technology to prolong both of these stages from occurring, with the initiation of the crack being the most investigated stage of the two for good merit. Through their research Liu et al. (2010) found that the time it takes for a crack to initiate may account for up to 80% of the total fatigue life of the component. This is highly dependent on the material toughness (Dowling, 2012). This implies that for an open crack, there is a limited amount of time before the component fails. Because of this, the possibility of retarding the initiation and/or the propagation of a crack, thus increasing the fatigue life performance, is appealing and has resulted in the development of multiple techniques. These techniques include shot peening, laser shock, interference fitting, and cold expansion (Fu et al., 2015). A summary of the former three techniques as well as an in-depth investigation into cold expansion follows next.

Shot peening is the process of bombarding a component surface with small spherical shot, often made of metal, glass, or ceramic particles. The bombardment creates small dimples on the surface of the component building compressive stress regions under the dimples (Dowling, 2012). A diagram of how the process of shot peening occurs and the region that is created can be seen in Figure 1.1. Through their research Fu et al. (2015) found that shot peening creates a surface roughness that can offset the improved fatigue performance caused by the residual stress regions. This offset leads to shot peening being a less viable option as a hardening technique.

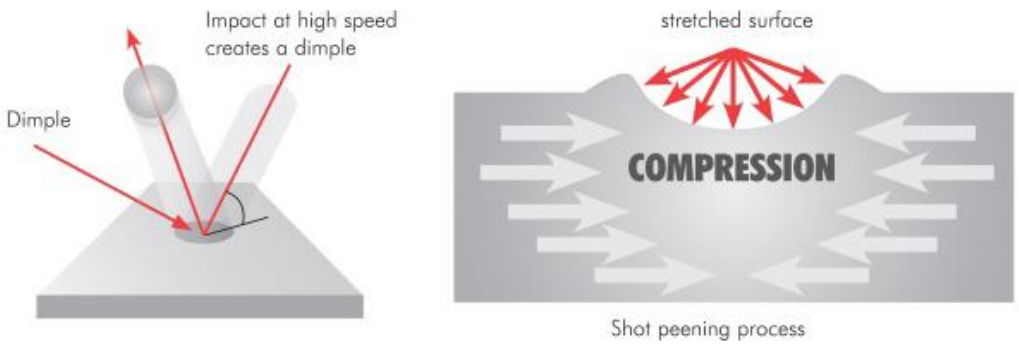

Figure 1.1 Shot peening process (Curtiss-Wright, 2018).

Laser shock or laser shock peening (LSP) uses the mechanical effects of a shockwave imparted by a laser pulse fired onto the component to create a residual stress region beneath the surface of a component, thus increasing the fatigue performance of said component (Antunes & de Oliveira, 2015). However, this method is costly in both the laser technology as well as operation cost for it to see significant use in the aircraft manufacturing process (Fu et al., 2015). A diagram of the process of LSP can be seen in Figure 1.2 showing how the shockwave propagates through the material (Birnbaum et al., 2010).

Interference fitting, also called press fitting, is the process of pressing a bolt, rivet, or bushing that has a larger diameter dimension than the hole in the component, thereby creating a tight combination through friction. This process is often produced with a hydraulic press that applies a large amount of force to ensure the compactness of the fit. This forceful insertion of a larger fastener creates the residual stress region leading to an improved fatigue life (Kim & Kim, 2019).

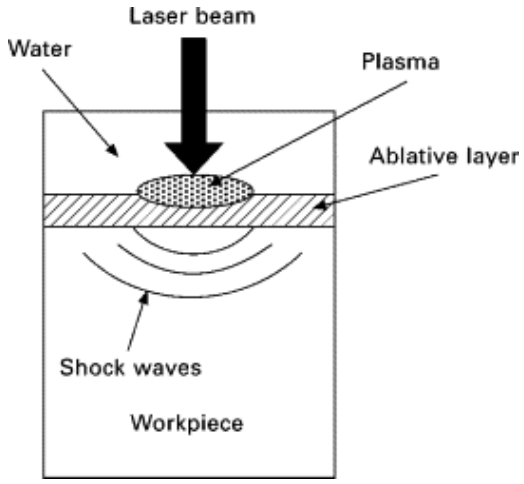

Figure 1.2 Diagram of Laser Shock Peening (Birnbaum et al., 2010).

Like the other two methods discussed previously, there are drawbacks that limit these hardening methods used in the aircraft manufacturing industry. These limitations as described by Fu et al. include the lack of ability to control the degree of interference applied, if the interference degree is too high it could lead to damage to the hole surface, also hole protuberance caused by the process can affect the strength of joints. The drawbacks of these methods have led to the focus of this research, cold expansion to become the primary use of toughening in the aerospace industry.

1.2. Overview of Cold Expansion

The most widely used hardening process to improve local toughness in the aerospace industry for over the last 30 years has been cold hole expansion (Mostefa et al., 2012). First developed by The Boeing Company (Chicgao, IL) during the 1970s, it has seen major usage on many different platforms of aircraft from military to commercial (Fu et al., 2015). The process of cold expansion is rather simple but the science behind what is ongoing throughout the process is quite complex. This section will analyze the main

processes to accomplish cold expansion as well as the science and formulation that bring to light the phenomenon accomplished by cold expansion.

The cold expansion process consists of inserting an oversized tapered mandrel into the fastener hole and then forcefully pulling the mandrel through the hole (Wang et al. 2017; Chakherlou & Vogwell, 2003). A diagram detailing the process of cold expansion can be seen in Figure 1.3 (Leon, 1998). The tapered mandrel may be combined with a lubricated sleeve that is draped over the mandrel. When the thickest part of the mandrel is pulled through the fastener hole the summation of twice the sleeve thickness and the mandrel diameter are greater than that of the hole diameter leading to the expansion.

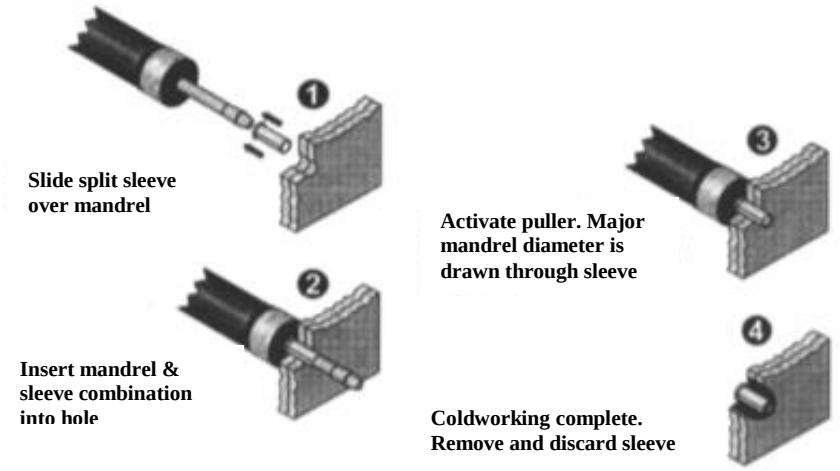

Figure 1.3 Diagram detailing the split sleeve cold expansion process (Leon, 1998).

This convention can be represented in Equation 4 where D_m is the diameter of the mandrel, t_s is the thickness of the sleeve, and D_{in} is the diameter of the fastener hole.

$$D_{in} < D_m + 2t_s \tag{4}$$

It is claimed that the forceful drawing through the fastener hole creates a residual compressive stress region that “inhibits the growth of and propagation of cracks” (Pasta,

2007, p. 1525). While the mandrel is being pulled through the fastener hole the material close to the edge of the hole becomes expanded plastically (Wang et al., 2017). This implies that the stress experienced by the material around the hole exceeds that of the limit yield stress of the material leading it to local plastic deformation. However, the material farther away from the hole does not experience the same level of stress and is therefore only elastically deformed (Wang et al., 2017).

Once the mandrel has been removed and there is an absence of applied stress, the portion of the material farther away from the hole that only experienced elastic deformation has a tendency to return to its original position. This "snapping back" of the elastically deformed material imposes a compressive stress on the plastically deformed material, creating the compressive stress region around the hole. This compressive stress region as mentioned above, "tends to cancel the stress resulting from external loading thus reducing the stress concentration area at the hole" (Liu et al., 2008, p. 271).

The residual compressive stress region has the potential to "extend approximately one radius from the edge of the hole" depending on the material and the degree of expansion (Leon, 1998, p. 1). This degree of expansion is related to the difference between the hole diameter and the mandrel diameter and the sleeve thickness, typically reported in percentage. The computation for the cold hole expansion can be seen in Equations 5 and 6, without and with split-sleeve respectively. The degree is also related to the percent strain that is experienced by the material during the cold expansion process. Liu et al. (2008) state that "in the aerospace industry a cold expansion degree between 2 and 6 % is typically used" (p. 271).

$$CE\% = \frac{D_m - D_{in}}{D_{in}} \cdot 100\% \tag{5}$$

$$CE\% = \frac{(D_m + 2t_s) - D_{in}}{D_{in}} \cdot 100\% \quad (6)$$

There are quite a few different methods that are used to apply cold expansion to a fastener hole, and these are hole edge expansion, direct mandrel expansion (sleeveless), ball expansion, and split sleeve expansion (Fu et al, 2015). These methods will be explained and reviewed beginning with hole edge expansion.

Hole edge expansion is the process of using a tapered indenter to extrude or hammer the edge of the hole until it extends. This method has a drawback in that the middle of the hole wall does not experience any of the benefits of a residual stress region, meaning that this method can only be effectively used for sheet metals and not thicker plates (Fu et al., 2015). The method of hole edge expansion can be seen below in Figure 1.4.

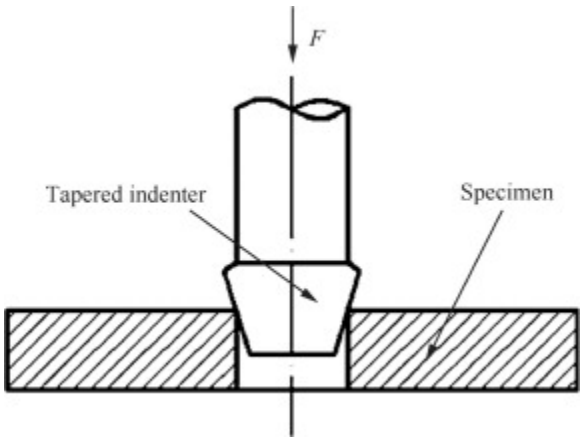

Figure 1.4 Hole edge expansion process (Fu et al., 2015).

Sleeveless cold expansion occurs in the same manner that was described above in the opening paragraph of this section. This method is rather simplistic, allowing it to become one of the more primary methods used in the industry. However this method has drawbacks. Contact between the mandrel and the surface of the hole creates friction and

this friction leads to surface damage that actually reduces the residual compressive region by a margin thus reducing the crack growth retardation benefits (Broek, 1989). Another limitation of this process is the need to access the parts from both sides, which is not suitable for closed pre-assembled structures like aircraft components.

The ball expansion process involves inserting a lubricated oversized steel ball into one side of the component and then removing it from the other side (Fu et al., 2015). Through their research Fu et al. (2015) found that the friction in this method is less significant than the mandrel only process because of an interference ring between the ball and the hole surface that is created; however, the benefits provided in fatigue performance are less in comparison to the other methods. Because of this, it is recommended that the ball expansion method be done twice from both directions in order to increase the residual stress region, which increases the time and cost in the aircraft manufacturing process. A diagram showing the ball expansion process can be seen below in Figure 1.5.

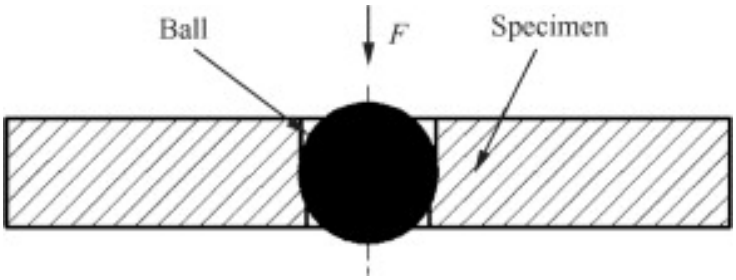

Figure 1.5 Ball expansion process (Fu et al., 2015).

The split sleeve method shown earlier in Figure 1.3, has the advantages of good adaptability, high efficiency as multiple can be done in very quick succession, and it causes little damage to the surface of the hole. It also requires access to only one side of

the component. Because of these advantages, this final method of cold expansion has been more widely used in the aerospace industry and is the process that was used for this research (Gopalakrishna et al., 2010). A second diagram detailing showing the assemblage of the split-sleeve tapered mandrel can be seen in Figure 1.6. This diagram provides good imagery as to how the cold expansion will be conducted here, as well as detailing the mandrel entry and exit face that will be mentioned in Chapter 2.

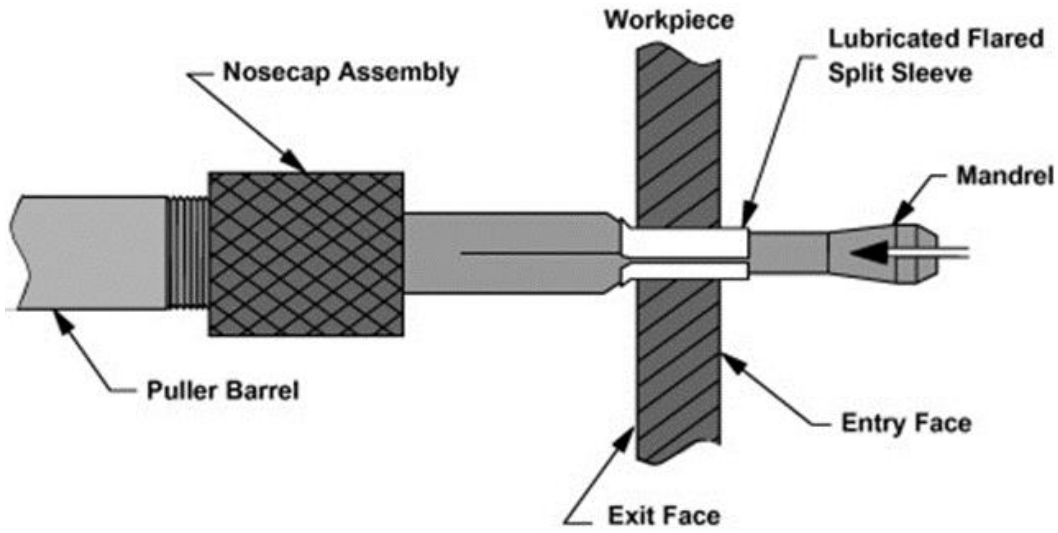

Figure 1.6 Diagram of the split-sleeve tapered mandrel assembly that will be used as the cold expansion method for this research (Burlat et al., 2008).

1.3. Motivation and Scope of Thesis

The development of a crack due to fatigue can occur at any stage in the lifetime of an aircraft. If a crack occurs, replacement or repair is necessary to recover the airworthy condition of the component. The simple replacement of fasteners, such as bolts or rivets, in the field, may cause oversized holes from typical maintenance procedures of primary structures. Once re-drilled or reamed, the oversize hole already has a fatigue history and small cracks may be present. One question still not answered is what would be the impact

of the cold expansion of holes containing micro or small cracks. Therefore, the motivation for this thesis is to examine if the known fatigue life benefits of the cold expansion of a fastener hole at the manufacturing stage can provide any fatigue life improvement when applied to a fastener hole that already has a small crack present. The findings of this research could lead to an avoidance of grounding an aircraft that can still fly while also delaying the economic and time cost that comes when providing full-scale maintenance of an aircraft. A review of the scope of this thesis can be found in the following paragraphs.

In addition to what has been discussed in this chapter, a literature review examining the history and research developments that pertain to the topics of research in this thesis can be found in Chapter 2. Previous research and the corresponding findings related to the benefits garnered by the cold expansion of fastener holes will also be reviewed. Elastic-Plastic Theory that the cold expansion of fastener holes is primarily based on will be reviewed as well. Finally, a review of the finite element modeling methods that can be to accurately model the process of cold expansion and the results that came from these modeling methods can be found in Chapter 2.

Chapter 3 will detail the methods used to complete the scope of this thesis. This chapter will go step by step and in detail on the processes that were followed from the very conception of the research through its completion. The stages of the experiment that will be covered include dimensioning and manufacturing of the testing specimens, using Digital Image Correlation (DIC) to map the development of strain during the cold expansion process, finite element modeling (FEM) of the cold expansion process, and the fatigue testing of the specimens. This chapter will also detail the experimental apparatus,

the materials, and the experimental equipment that was used for each stage of the research.

The results from the different stages of the research will be presented in Chapter 4. Stress contours from the FEM during the cold expansion will be presented along with the strain contours that are found by the DIC. Images of crack growth during both the control sample and the experimental sample will be included in this chapter along with images of the fracture surface of both specimens.

Based on the results presented in Chapter 4, the main conclusions of this research can be found in Chapter 5. These conclusions will either verify or deny the impact that cold expansion of fastener holes with initial cracks present at the hole edge. Conclusions will also be made based on the results of the FEMAP simulations and DIC analysis as appropriate methods to examine the cold expansion application. Potential future works that can build on the research presented in this thesis or lead to improvements in the procedure and results provided in this thesis will also be presented in Chapter 5.

2. Review of Literature and Theory

Investigations into fatigue and the technology that can be used to overcome the negative effects that result from fatigue have gone on for more than 60 years of the aerospace industry. With academic researchers and industrial companies, such as The Boeing Company, and professionals alike looking at ways to counteract and even prevent fatigue crack growth. This chapter will chronicle the development of research and the history of previous research involving cold expansion using the mandrel method. Another important focus regarding cold expansion is developing effective modeling of the expansion process. This modeling has been used to develop a deeper understanding of the residual stress region that is created after the expansion. A literature review on the different simulation techniques, using finite element software, that have been implemented will be conducted in the following section as well. In addition to a review of relevant literature, a review of relevant theory, Elastic-Plastic theory that applies to the cold expansion process will be completed in this section. This theory discusses the physical happenings that are occurring during the cold expansion process and can also be used as a predictor of how the compressive residual stress region will develop.

2.1. Review of Literature on Cold Expansion

Phillips (1974) is most notable for performing early investigations into the effects of cold expansion, in particular the split-sleeve technique. Throughout his research he focused on a 21-month two-stage investigation that developed an optimized process that takes into account the different parameters leading to effective cold expansion using the split-sleeve method. In the first stage of Phillips investigation, parameters such as mandrel taper angle, percentage of cold expansion, design of the sleeve and its lubrication method, required puller force, and requirements for reaming after the

application of cold expansion were explored. In the second phase, Phillips examined the effects of prior hole processing, orientation of the split-sleeve, and countersinking of the hole, has on the fatigue life of a component by performing fatigue testing on coupon specimens of steel, aluminum alloys, and titanium alloys. The most significant result that Phillips found was that if the hole was reamed after the cold expansion was applied, the fatigue life benefits provided by the cold expansion is reduced, with some levels of reaming even removing any benefits of fatigue life in total.

Chakherlou and Vogwell (2003) examined the effects that mandrel only cold expansion had on the fatigue life of specimens. This investigation was carried out by using a sinusoidal constant amplitude loading where the loading stress ratio, R, was at a value of zero. As expected, the specimens that underwent cold expansion saw fatigue life improvement of nearly ten times as compared to the simply drilled specimens. Chakherlou and Vogwell (2003) reported that fatigue life featured a more significant improvement when the specimens underwent low alternating stresses as opposed to high alternating stresses. A graphical representation of Chakherlou and Vogwell's findings can be seen in Figure 2.1. It was also found by analyzing fracture surfaces after specimen failure, that the initiation of cracks were found on the side of the specimen that the mandrel entered through, while for the specimens that were simply drilled, the cracks initiated at the mid-plane of the specimens.

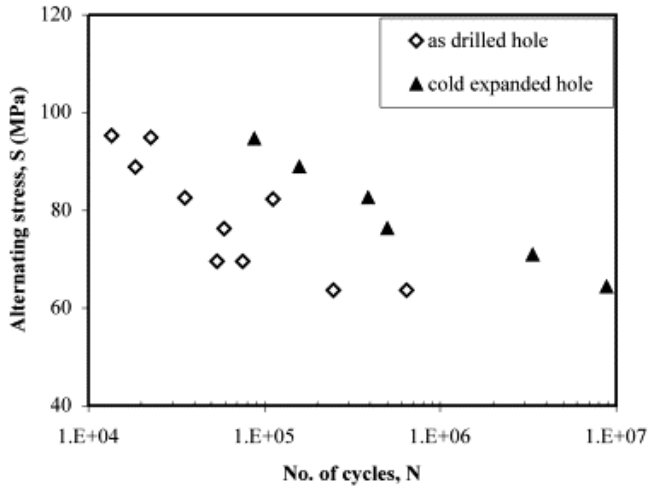

Figure 2.1 Fatigue cycle results of specimens at varying alternating stress levels (Chakherlou & Vogwell, 2003).

Zhang and Wang (2003) examined improvements in fatigue life that cold expansion has on specimens that have already experienced some level of fatigue as opposed to applying cold expansion at the manufacturing stage. The experiment consisted of an Al 2024-T351 low-load transfer joint that had been pre-fatigued from 25% to 75% of the baseline fatigue life for fastener holes. A standard flight-by-flight loading sequence, FALSTAFF spectrum, was used to load specimens until failure or a certain percentage of the baseline fatigue life. Zhang and Wang (2003) found that while applying cold expansion to the specimen at any stage of the fatigue life, the benefits of the expansion are still present, Figure 2.2. It was also found that there was a reduction in the time it took to initiate a crack when the previous cumulative fatigue life was above 25%. Similar to Chakherlou and Vogwell (2003) research, Zhang and Wang (2003) also found that the critical cracks ultimately developed at the face that the mandrel was input through, citing that the residual compressive stress region is lower at this entry face than at the exit face.

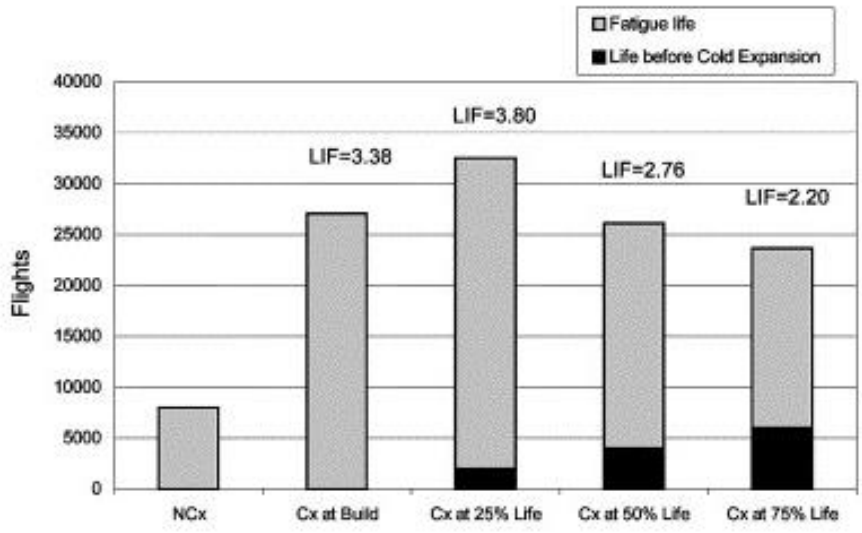

Figure 2.2 Ultimate fatigue life of specimens that have undergone cold expansion at a varying percentage of fatigue life (Zhang & Wang, 2003).

Liu et al. (2008) investigated the development of residual stress regions as well as the effect that different percentages of cold expansion have on the fatigue performance of components composed of aluminum alloy 2A12T4. The observation of residual stress development throughout the cold expansion process was conducted using an X-ray technique to measure surface residual stresses on the mandrel entrance face. Specimens with cold expansion percentages of 2%, 4%, and 6% were fatigued with a constant amplitude sinusoidal loading and an R of 0.1. Liu et al. (2008) found that the development of the tangential residual stress region was non-axisymmetric in nature with the non-axisymmetric development being more evident as the cold expansion percentage increased. Also, it was found that the higher cold expansion percentage, 6%, developed the best performance, achieving six times the fatigue life of the non-cold expanded specimens.

Gopalakrishna et al. (2010) examined the effect that two different spilt-sleeve cold expansion methods, tapered mandrel, and ball techniques, had on the fatigue performance of Al 2024-T3 expanded holes with varying levels of expansion percentages. The development of the residual stress regions during the cold expansion was monitored with strain gauges, one gauge to monitor radial development, and three to monitor tangential strains. After applying a variety of expansion percentages to the holes, Gopalakrishna et al. (2010) found that for both cold expansion methods the development of residual stress regions was found to decrease for the 6% cold expansion specimens. The drawbacks of the reduction were confirmed by the fatigue testing which showed that the fatigue life improvements decreased when compared to the 5% expansion, this can graphically be seen in Figure 2.3. It was also found after fatigue testing, that the tapered mandrel method delivered significantly better results as compared to the split-sleeve ball, with fatigue life being 200% greater. The results of this investigation show how effective the tapered mandrel cold expansion method is for improving fatigue life.

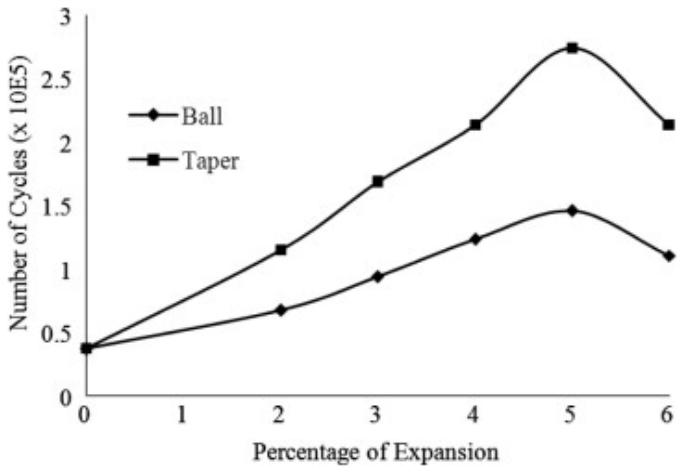

Figure 2.3 Results of fatigue experimentation with two methods of cold expansion application. Showing the decrease in performance after 5% expansion and the superiority of the tapered mandrel method (Gopalakrishna et al., 2010).

Wang et al. (2017) investigated the fatigue performance of cold expanded holes of 6061-T6 aluminum alloys. After applying a 4.0% cold expansion to the specimens, they were then loaded under tension-tension loading with an R of 0.1 and a frequency of 12 Hz. It was determined that a fatigue life improvement of 247% occurred for the cold expanded holes as opposed to the non-cold expanded holes showing the benefits that can be gained by expansion. One important discovery after examining the fracture surface with a Scanning Electron Microscope (SEM), is that the fatigue cracks bypass what is determined to be a tri-directional compressive stress region. This tri-directional compressive region was determined to be formed by the internal residual stresses created by the cold expansion and the external loading of the fatigue testing. By examining the fracture surface of the specimen with an SEM, Wang et al. (2017) found that growing cracks had to navigate around the tri-directional compressive stress regions which led to longer fatigue life before the crack reached critical length. Wang et al. confirmed that the compressive region is the main cause of the improvement in the fatigue life of the cold expanded samples.

2.2. Review of Literature on Finite Element Modeling

Kang et al. (2002) developed a simplified finite element simulation of the cold expansion process in two different aluminum alloys, Al 2024-T351 and Al 7050-T7451. The method by Kang et al. applies a uniform displacement to the nodes on the hole-edge that mimics the 4% expansion that was desired for the investigation and then simulates the removal of the mandrel by removing the applied displacements. A quarter of the experimental specimen was modeled using ABAQUS (Providence, RI) 5.8/CAE code, because of the inherent symmetry of the specimen. Using this method, Kang et al. (2002) found that plastic deformation develops in a similar method as to be expected throughout

the surface of the hole. Following the simulation, the analysis showed that the residual stress field has variations in magnitudes through the thickness of the hole which is similar to what was found in the experimental test discussed in Section 2.1. The development of strain using this simulation method also showed a good comparison to experimental measurements showing viability of this simulation method.

Mahendra Babu et al. (2008) suggested a different simplified method to accurately simulate the cold expansion process using finite element software. This method, as defined by Mahendra Babu et al. (2008), radially expands the fastener hole with applied displacements one layer at a time until the entire thickness of the hole in Al 2024 has been expanded and then repeats this process to simulate the removal of the mandrel. The modeling involved using a quarter of the specimen due to symmetry. Using this method provides the benefit of simplicity while also providing the opportunity to capture the variation of the residual stress regions through the thickness of the hole. With a comparison to published values, Mahendra Babu et al. (2008) found the suggested method of cold expansion simulation featured similar values as that of experimental values, also showing this method as a viable option. Mahendra Babu et al. (2008) also found that this suggested method provides a more realistic simulation than simple displacement conducted by Kang et al. (2002).

A different method of modeling the cold expansion process was conducted by Houghton in 2010. Houghton modeled the cold expansion of a hole in a plate of Al7075-T651 by using the ABAQUS 6.9EF modeling software. The new method involved modeling the rigid mandrel and elastically deformable split-sleeve with the mandrel being axially pulled through the hole to create a 4% expansion. The results of this simulation confirmed that the peak compressive stress regions occur on the surface of

the plate with a minimum stress development at the mid-thickness as found in the other methods. However, modeling the physical pulling of the mandrel through the sleeve and the hole revealed that there was a more complex development of residual tangential stress regions that cannot be seen with uniform expansion methods. Through his research Houghton (2010) found that this more complex development shows that the contact that sleeve and mandrel make with the hole surface has an impact on the development of the residual stress region. One noted drawback of this method is that it is more complicated to model and more computationally involved.

Yasniy et al. (2017) modeled the cold expansion of holes in Al 2024-T3 dogbone samples using the modeling software, ANSYS Explicit Dynamics. Similar to Houghton (2010), Yasniy et al. (2017) modeled the mandrel as a rigid surface and had the mandrel being physically pulled through the hole in the plate as the method of expansion. A range of expansion percentages from 1 to 3, showed that the maximum residual stress, σ_{yy}^{res}, developed a maximum value at the mid-thickness of the plates as opposed to this particular area showing the minimum residual stress development as found by Houghton (2010). It was found by simulating the three different expansion percentages, the ratio comparing the compressive stress regions at the mid-thickness to the same region on the entry face decreases to almost a 1:1 ratio at a 3% expansion.

El Habiri et al. (2018) also conducted simulation of cold expansion of a hole in a plate of Al 2024-T351 using ANSYS software. The meshing of the quarter plate of the specimen was conducted using the automatic tetrahedral meshing generator provided by ANSYS which yielded a coarser and less uniform mesh than found in previous literature. El Habiri et al. (2018) also modeled a tapered mandrel to simulate the cold expansion process by incrementing the nodal positions of the mandrel in the -Z direction. In

addition to the mandrel being displaced through the hole, the nodes on the surface of the hole had an incremental pressure loading. The analysis of this simulation of cold hole expansion showed similar findings with the development of residual stress regions as found in other studies. Through their research El Habiri et al. (2018) found that the residual stress region on the exit face of the specimen showed the highest residual stresses throughout the thickness of the specimen. It is believed by this simulation, that the induced friction between the plate and the mandrel provides a beneficial effect in the development of the tangential residual stress region and is what leads to the nonuniform through-thickness development.

2.3. Elastic-Plastic Theory

One way to predict the development of residual compressive stress regions around the hole edge after the removal of the mandrel and split sleeve follows the theory of isotropic plasticity, based on work hardening as proposed by D.C. Drucker (1951) and with the ideal plasticity equations presented by Y.C. Fung (1965) for an elastic perfectly plastic material. The theory and equations that relate to this development for plane stress conditions will be reviewed in this section. The radius of the plastic zone, *c*, that is developed because of the cold expansion process can be found by iteratively solving Equation 7 below,

$$U_m = \frac{(1-\nu)\tau_y c^2}{Ga} - \frac{(1-2\nu)P_c a}{2G} - \nu\varepsilon_2 a \tag{7}$$

where U_m is the radial displacement produced by the mandrel. ν is the material property poison ratio, τ_y is the shear yield stress using the Tresca Criteria for failure, Equation 8. G is the shear modulus of the material, Equation 9, a is the radius of the fastener hole, P_c is the internal pressure required to cause the yielding to reach the plastic zone radius,

Equation 10. ε_2 is the axial strain, experienced by the area around the hole when it becomes plastically deformed, Equation 11.

$$\tau_y = \frac{\sigma_Y}{2} \tag{8}$$

Here, σ_y is the yield stress or limit stress of the material. This stress is the level at which the component will begin to plastically deform.

$$G = \frac{E}{2(1+\nu)} \tag{9}$$

Here, E is Young's modulus of the material and shows how elastically stiff the material is when loaded.

$$P_c = \tau_y \left[1 - \frac{c^2}{b^2} + \ln\left(\frac{c^2}{a^2}\right)\right] \tag{10}$$

Here, b is half of what is called the system external diameter, or the distance from the center of the hole to the closest external edge of the component.

$$\varepsilon_2 = -2\nu\left(\frac{a^2}{b^2 - a^2}\right)\frac{P_c}{E} \tag{11}$$

While the mandrel is being removed and the component is being unloaded, there will be a reverse yielding around the hole. Two conditions must be met in order for reverse yielding to occur as listed below.

1. $\frac{b}{a}$ must be greater than 2.22, which is a condition for the minimum value of edge distance as defined in good design practices (Niu, 2011).

2. $(2 * P_{Y_i}) < P_c < P_{Y_f}$ from necessary boundary conditions as proposed by Drucker (1951).

Where P_{Y_i}, is the pressure required to yield the material due to pure shear stresses, Equation 12. P_{Y_f} is the internal pressure that is required to cause full yielding of the plastic region, and can be seen formulated in Equation 13 below.

$$P_{y_i} = \tau_y \left(1 - \frac{a^2}{b^2}\right) \tag{12}$$

$$P_{y_f} = 2\tau_y ln\left(\frac{b}{a}\right) \tag{13}$$

Understanding the terms in condition 2, it becomes obvious why it is a stipulation on reverse yielding; because if the pressure required to yield the material to the plastic zone radius, c, is greater than the pressure which causes full yielding, than the material around the hole would be fully yielding.

If the conditions above are met, then the radius of the reverse yielding process, r_y, can be found by using Equation 14. The radius can be found by iteratively solving for r_y.

$$r_y = 2\left[\frac{r_y^2}{b^2} - ln\left(\frac{r_y^2}{ac}\right)\right] - \frac{c^2}{b^2} - 1 \tag{14}$$

When the mandrel is fully removed there will be an inward radial displacement around the hole. This inward displacement is caused by the reaction of the nearby material that was only elastically deformed, forcing the inner portion to revert to its original position. This inward radial displacement will be inherently negative because it will be opposing the displacement caused by the cold expansion. It is important to notice that even with this inward displacement, the final hole diameter will be greater than the

original diameter because of the fully yielded region on the hole surroundings, i.e. $|U_m| > |U_{in}|$. The formulation for the inward radial displacement can be seen in Equation 15.

$$U_{in} = -\frac{P_c a}{E}\left[\left(\frac{b^2 + a^2}{b^2 - a^2}\right) + \nu\right] \tag{15}$$

The residual stress that is developed, tangential, σ_t, and radial, σ_r, after the cold expansion process can be formulated as a function of the distance away from the edge of the hole, r. This development can be broken into three distinct sections based on how far away from the hole the stresses are desired. These three distinct regions are the plastic region, the reverse yielding region, and the elastic region.

The radial residual stress, Equation 16a, and tangential residual stress, Equation 16b, for the plastic zone is to be used for, $a \leq r \leq r_y$:

$$\sigma_{r_{pl}}(r) = -\tau_y\left[1 - \frac{c^2}{b^2} + ln\left(\frac{c^2}{r^2}\right)\right] + 2\tau_y\left[1 - \frac{r_y^2}{b^2} + ln\left(\frac{r_y^2}{r^2}\right)\right] \tag{16a}$$

$$\sigma_{t_{pl}}(r) = \tau_y\left[1 + \frac{c^2}{b^2} - ln\left(\frac{c^2}{r^2}\right)\right] - 2\tau_y\left[1 + \frac{r_y^2}{b^2} - ln\left(\frac{r_y^2}{r^2}\right)\right] \tag{16b}$$

The radial residual stress, Equation 17a, and the tangential residual stress, Equation 17b, for the reverse yielding region is to be used for, $r_y \leq r \leq c$:

$$\sigma_{r_{ry}}(r) = -\tau_y\left[1 - \frac{c^2}{b^2} + ln\left(\frac{c^2}{r^2}\right)\right] + \frac{2\tau_y r_y^2}{b^2}\left[\frac{b^2}{r^2} - 1\right] \tag{17a}$$

$$\sigma_{t_{ry}}(r) = \tau_y\left[1 + \frac{c^2}{b^2} - ln\left(\frac{c^2}{r^2}\right)\right] - \frac{2\tau_y r_y^2}{b^2}\left[\frac{b^2}{r^2} + 1\right] \tag{17b}$$

The radial residual stress, Equation 18a, and the tangential residual stress, Equation 18b, for the elastic region is to be used for, $c \leq r \leq b$:

$$\sigma_{r_{el}}(r) = -\frac{\tau_y c^2}{b^2}\left(\frac{b^2}{r^2} - 1\right) + \frac{2\tau_y r_y^2}{b^2}\left[\frac{b^2}{r^2} - 1\right] \tag{18a}$$

$$\sigma_{t_{el}}(r) = \frac{\tau_y c^2}{b^2}\left(\frac{b^2}{r^2} + 1\right) - \frac{2\tau_y r_y^2}{b^2}\left[\frac{b^2}{r^2} + 1\right] \tag{18b}$$

It should be noted that for Equations 16a, 17a, and 18a, the proper sign for compressive stress is negative. This negative stress value shows that the region developed around the hole will be compressive in nature, which is to be expected after discussing what is physically happening during the cold working process. Another thing to note is that the tangential residual stress is the more important of the two residual stresses for the point of view of fatigue because this is the stress acting perpendicular to the crack. The loading is naturally perpendicular to the radial direction meaning the tangential residual stress is what counteracts the service applied stress, improving the fatigue life of the component. Depending on the initial crack size and level of cold expansion, the crack will have to grow through the compressive stress zone, which leads to an increase in fatigue life or even the crack arrest, if the compressive stress zone is high enough.

3. Methodology

The process of this thesis can be broken down into two distinct stages, preparation and experimentation. The preparation stage involved dimensioning and manufacturing specimens for experimentation and also verifying calculations used for dimensioning by using Digital Image Correlation and Finite Element Modeling. The process and equipment that were required to complete the preparation stage will be discussed in this chapter.

The experimentation stage of this research consisting of two fatigue tests, one with a specimen as it was manufactured and one with cold expansion. The process and the equipment that was required to complete the experimentation stage will be reviewed in this chapter. First, a review of the material of the tested specimens.

3.1. Specimen Material

In the aerospace industry, it is important to choose a material that provides high strength while also maintaining relatively low weight. Because of this, a majority of aircraft structures are primarily composed of aluminum alloys (Mello et al., 2016), with the most widely used alloy being Al 2024-T3 or the “aircraft alloy.” Al 2024-T3 is typically chosen for applications that require a high strength-to-weight ratio and also very good fatigue resistance (Dowling, 2012). This has led to Al 2024-T3 being primarily used for fuselage and wing components along with other aircraft structures. The chemical composition of Al 2024-T3 can be seen in Table 3.1. Material properties of the alloy are required for FEM simulations as the software uses these properties when making respective calculations. It is also necessary to have material properties for classical plasticity analysis as presented in the previous chapter. A summary of material properties

that were used for FEM simulations can be seen in Table 3.2 with most properties coming from MIL-HDBK-5J (DOD, 2003).

Table 3.1

Chemical composition of Al 2024-T3 alloy used for experimentation.

Element	**Al**	**Cu**	**Mn**	**Mg**
Weight (%)	93.5	4.4	0.6	1.5

(Gopalakrishna et al, 2010)

Table 3.2

Material properties of Al 2024-T3 alloy used for experimentation.

Property	**Value**
Young' Modulus, GPa (ksi)	72.4 ($10.5\ x\ 10^3$)
Plasticity Modulus, GPa (ksi)	0.607 (88.0)
Yield Strength, MPa (ksi)	324 (47.0)
Ultimate Strength, MPa (ksi)	441 (64.0)
Poison ratio	0.33
Density, g/cm^3($lb./in^3$)	2.78 (0.10)

(DOD, 2003)

As a simplification, the material in the FEM software was defined as bi-linear elastic-plastic, meaning that both the elastic and the plastic regions of the material are linear with both slopes of these linear portions being important moduli. The first being the Young's Modulus as provided in Table 3.2. The Plastic Modulus had to be obtained from a full stress-strain curve. It can be easily determined by mapping individual points along the stress-strain curve of Al 2024-T3, which can be found in Appendix A, and then finding the slope of the plastic region of the curve. The mapping of the individual points can be seen in Figure 3.1. The longitudinal curve shown in Figure 3.1 was used for

mapping the rolling direction of the material as well as for being the typical loading direction.

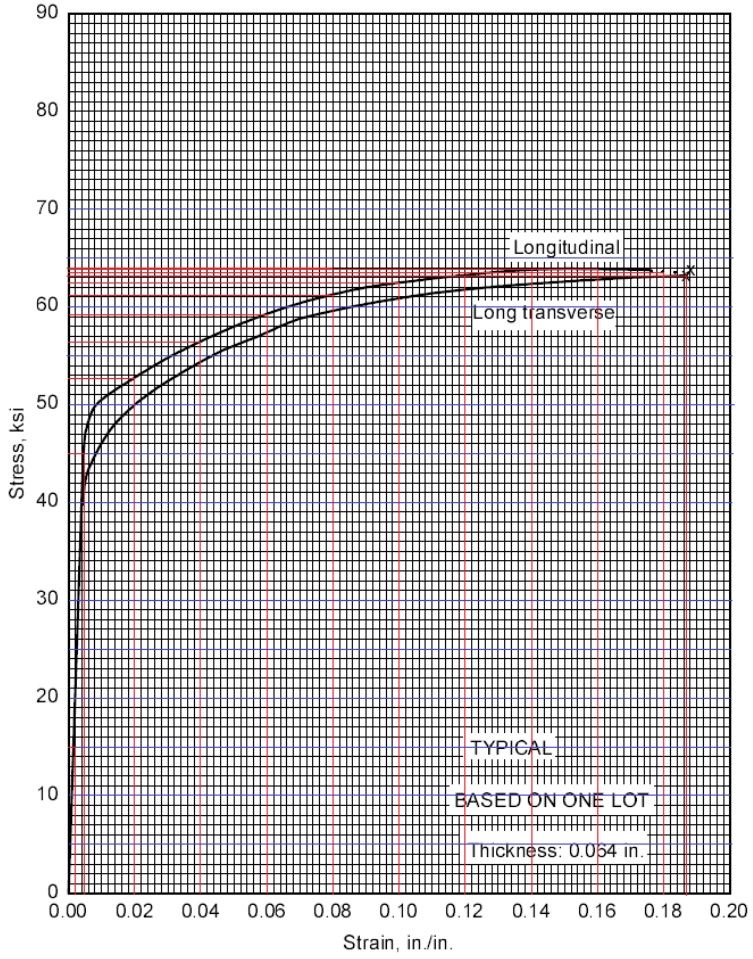

Figure 3.1 Typical tensile stress vs. strain curve for Al 2024-T3 showing mapping (red lines) to determine the Plasticity Modulus used for FEM simulations (Rice et al., 2016).

3.2. Dimensioning and Manufacturing of Experimental Specimens

Dimensioning the experimental specimens was a vital step in the overall process of this research. The Elastic-Plastic Theory detailed previously was used to ensure that appropriate dimensions were used to not inhibit benefits of cold expansion. Essentially, if the specimen width is too narrow, then the edge of the specimen will interact with the residual stress region that is created by cold expansion. This interaction will lead to a

degradation in the performance of the residual stress region and reduce benefits that cold expansion would provide. Also, the convention in the aircraft industry when designing a component that will have fastener holes is that there should be an edge distance from the edge of the fastener hole to the edge of the component of around three times the radius.

A combination of industry convention and examining where the residual stress region zeroes out, lead to finding the minimum width dimension that experimental specimens should conform to. Note, after taking into account the factors that the specimen width depends on, the width of experimental specimens also took into account the ease of manufacturing. The length dimension of specimens was determined in a way to have adequate material that can be gripped by the tensile testing machine and homogenize stress in the gauge section. It is worth noting that length was also dimensioned to ease their manufacturing.

Dimensioning of the fastener hole size that would be drilled into the specimen is dependent on two factors. The first factor is the desired cold expansion percentage be within the accepted industry range. As seen in Equation 6, the cold expansion percentage depends on three parameters: mandrel diameter, sleeve thickness, and fastener hole diameter. Only the hole diameter was able to be manipulated, because the mandrel diameter and sleeve thickness were restricted to available mandrel tool and split-sleeves. Because of this limitation, the fastener hole diameter was partly dimensioned based on the desired cold expansion parameter. The second factor that led to the fastener hole diameter sizing is the ability to conform to traditional drill bit sizing. There are common drill bit sizes that are readily available and would be found in the industry, so conforming to sizes similar to what is found in industry was decided. It is also worth noting that the thickness of experimental specimens was determined by the thickness of the provided Al

2024-T3 sheet. The respective dimensions for the experimental specimens can be found in Table 3.3 below.

Table 3.3

Relevant experimental specimen dimensions.

Specimen Dimension	**Value, cm (in.)**
Length	25.4 (10.0)
Width	5.715 (2.25)
Thickness	0.3175 (0.125)
Drill Diameter	0.754 $\left(\frac{19}{64}\right)$

Using dimensions listed in Table 3.3, engineering drawings of the specimen were produced and provided to the Embry-Riddle Aeronautical University Manufacturing Shop for production. Ten samples that would be used for cold expansion experimentation, DIC experimentation, and finally fatigue testing were fabricated. An example of the engineering drawing provided to the manufacturing shop is shown in Figure 3.2, with a full size image found in Appendix A. An image of a fabricated Al 2024-T3 experimental specimen is shown in Figure 3.3.

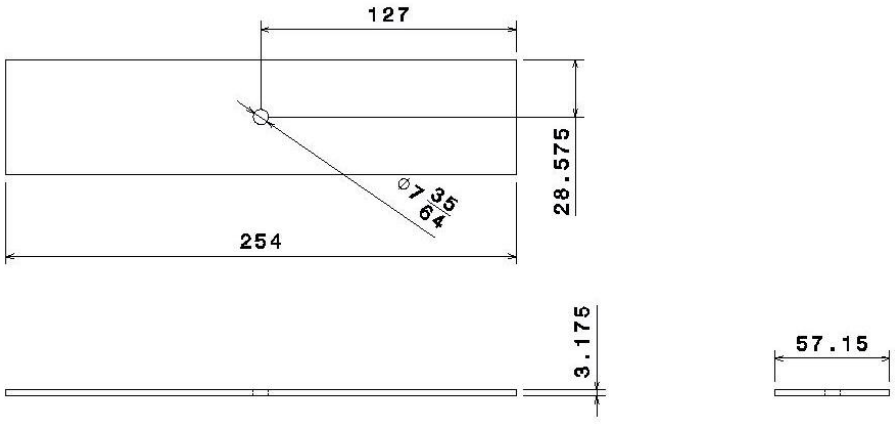

Figure 3.2 Engineering drawings of experimental specimen dimensions that were provided to the ERAU Manufacturing Shop.

Figure 3.3 Fabricated Al 2024-T3 experimental specimen.

3.3. Finite Element Modeling of Cold Expansion

The finite element modeling, FEM, of the cold expansion process was completed in three distinct stages using the FEM software FEMAP v11.4.2 with NX Nastran solver produced by Siemens (Munich, Germany), to verify and compare analytical computations using elastic-plastic theory. This division into stages was performed in a build-up method from less complicated modeling and simulation to more realistic. The three stages that FEM was divided into are two-dimensional linear static analysis, three-dimensional linear static analysis, and three-dimensional advanced non-linear static analysis. All three of these stages, to be detailed in the following sections, followed similar setup procedures which will be described below.

A three-dimensional model of the Al 2024-T3 experimental specimens was modeled using the modeling software CATIA V5-6R2017 with dimensions to match values found in Table 3.3. The geometry of the CATIA model was imported into FEMAP software for geometrical meshing and simulation. The material properties of Al 2024-T3 were input into the respective section, both linear and nonlinear properties. In addition, the stress-strain points that were found from mapping Figure 3.1 were also inputted into FEMAP so that the software had the stress-strain curve for a reference. It is important to

note that simulations at each stage of this modeling were a simplified version of the cold expansion process because the mandrel and sleeve being pulled through the fastener hole were not modeled. Instead, the cold expansion process was simulated by applying either nonzero constraints or surface pressures to the inside of the fastener hole surface like others (Kang et al., 2002; El Habiri et al., 2018).

3.3.1. Two-Dimensional Linear Static Modeling

The two-dimensional modeling was conducted by taking a mid-surface cut of the three-dimensional imported geometry. This simplified the modeling as well as verified results provided by analytical calculations before a more complicated and computationally involved simulation was conducted. The meshing of the geometry was conducted by applying the mapped meshing method. The geometry of a washer which maps, with pad included, were used around the fastener hole geometry to conform better to the curves of the hole. This conforming occurs by essentially having more curves around the hole geometry allowing for manipulation. Having this conforming around the hole surface allows for a finer meshing around the hole, this is important because a finer mesh allows for a more accurate calculation and leads to developing a better idea of the stresses and strains that are developing. Farther away from the edge of the hole, the fineness of the mesh is not as crucial, therefore the surface of the specimen was divided into distinct sections to allow for a coarser mesh to be applied to regions farther from the hole. The meshing around the fastener hole can be seen in Figure 3.4.

The boundary conditions for this two-dimensional simulation of the cold expansion process is slightly different than that of the other two simulations, this difference revolves around the fact that it is a two-dimensional surface. Because the surface is inherently flat, a surface pressure to the wall of the hole cannot be applied, therefore a new method

needed to be implemented. This new method involved applying a type of nodal constraint that is defined as “NonZero Constraints,” in FEMAP, which essentially applies a prescribed displacement to the selected nodes without having a load applied. This “NonZero Constraint” was applied to the nodes around the edge of the hole and had a value equal to the displacement equivalent to the mandrel diameter and the sleeve thickness in the radial direction. It is important to note that a cylindrical coordinate system was established at the center of the hole. This was required because FEMAP is inherently in the “xy” coordinate system so any “NonZero Constraint” would not be an appropriate value for nodes not along the x-axis.

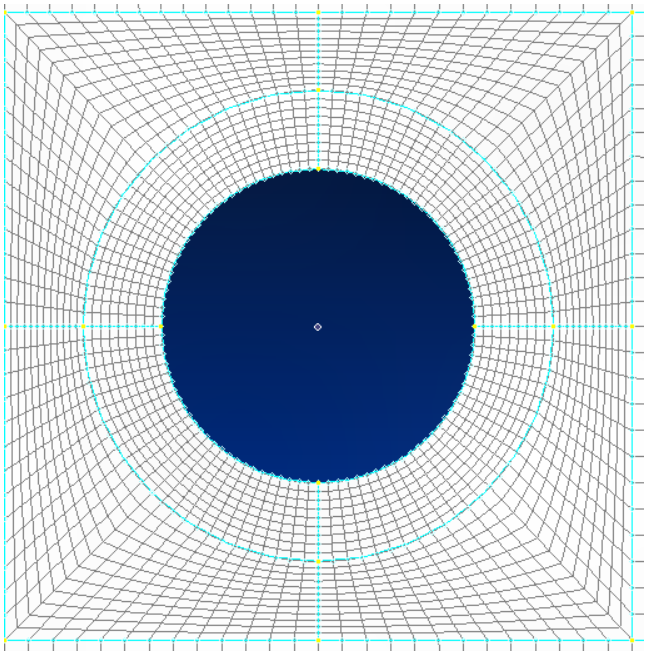

Figure 3.4 Meshing pattern around the fastener hole of the two-dimensional model.

In addition to the constraint applied to the inner curves of the fastener hole, fixed boundary constraints were applied to the top and bottom curves of the specimen. This constraint condition is similar to what a specimen will experience while in the tensile

testing machine when the cold expansion is applied, with the specimen unable to translate in the x, y, or z-axis, nor can it rotate about either of the axes. The simulation was conducted to determine if the deformation applied to the hole edge by the mandrel and sleeve would produce an adequate strain percentage. The results of this simulation will be discussed in Chapter 4.

3.3.2. Three-Dimensional Linear Static Modeling

The next step in the process of FEM simulation of the cold expansion process is a three-dimensional linear static simulation. As compared to the previous method, this step was more difficult as there were significant geometric modifications required in order to have a refined mesh along the hole edge such as in the two-dimensional modeling, while the third step used the geometry defined here. Similar to the two-dimensional simulation, a washer and pad was applied to the hole to allow for a refined mesh, this was done to both the front and back surfaces of the model. In addition to the washer and pad combination, the wall of the hole was divided into smaller sections to obtain the appropriate meshing of the system for the desired analysis resolution. Also, like the two-dimensional model, the surfaces of the model were divided to allow for coarser mesh farther away from the hole edge where the calculations were not as important.

To mesh the three-dimensional model, the FEMAP “Automatic Meshing” tool was used with tetrahedral elements, with solid properties, throughout the thickness of the model. The meshing tool was manipulated to allow for a better fit to the geometry, the options that were applied include: Quadratic Mesher; Jacobian Correction; Smooth Solid Elements; and Midside Nodes. The Quadratic Mesher meshes against the solid geometry and then maps the automatically generated mesh to the geometry more accurately, especially for curved surfaces, such as around the fastener hole.

Enabling the Quadratic Mesher option allows for the Jacobian Correction option to be enabled as well. This option uses a Jacobian algorithm to better map the meshing elements to the curve generated by the Quadratic Mesher. This is useful to better conform to curved surfaces such as the fastener hole. The Smoothing Solid Elements option introduces a defined tolerance, which FEMAP will adhere to when using solid elements to match curves, leading to a better representation of the present geometry by the solid meshing. The defined tolerance for the modeling of the experimental specimen geometry was 0.0001. The Midside Nodes on Surface option, like the other options defined above, improves the meshing performance of the Automatic Mesher by limiting the degree of angle distortion that any particular solid element is allowed to experience.

Once the automatic meshing was applied, manual refinement was conducted along the washer and pad geometries using the FEMAP "Meshing Toolbox." This toolbox allowed for the number of elements along a curve to be increased by a defined factor, thus providing a smaller and more refined mesh. It should be noted that the refinement using this method was applied along all curves of the model to ensure that there was a uniform mesh throughout the specific regions with no drastic changes of element size or shape, as is good practice of finite element modeling. The meshing pattern of the surface around the fastener hole can be seen in Figure 3.5.

After the meshing was refined to an acceptable amount, boundary conditions were applied. Similar to the two-dimensional simulation, fixed boundary constraints to the top and bottom surfaces of the model were applied to prevent any displacement or rotations of the six typical degrees of freedom. Note, these constraints were applied far away from the hole shown in Figure 3.5, so there is no direct interaction between the holes and the boundary constraints. Unlike the two-dimensional simulation, a surface pressure was

applied to the wall of the hole to simulate the mandrel and sleeve expanding the diameter of the fastener hole.

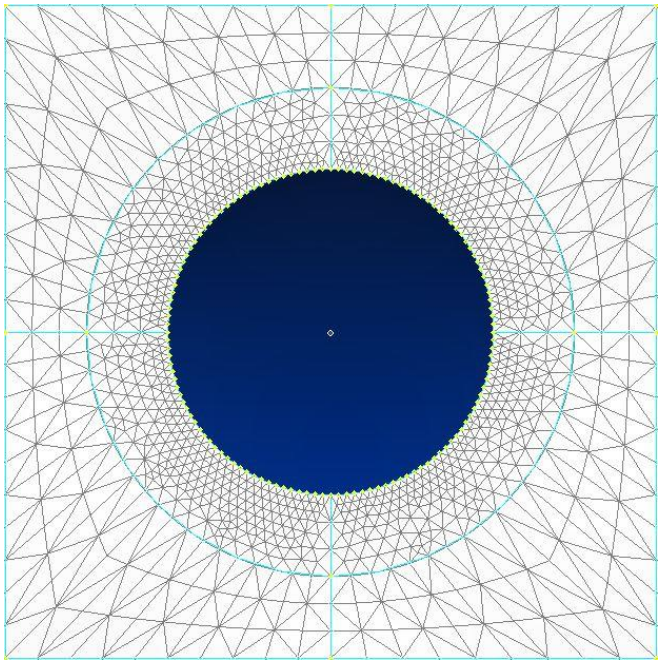

Figure 3.5 Meshing pattern around the fastener hole of the three-dimensional model

The applied surface pressure value was found iteratively by increasing the value of the pressure applied until an appropriate value of strain percentage and radial deformation was found. It should be noted that like the "NonZero Constraints" of the two-dimensional simulation, the surface pressure was linked to a created cylindrical coordinate system to ensure that the pressure was indeed applied in the correct radial direction. This simulation was conducted to examine the level of stress experienced with the application of cold expansion. The results of this simulation will be discussed in Chapter 4.

3.3.3. Three-Dimensional Nonlinear Static Modeling

The three-dimensional nonlinear static modeling of the cold expansion process was fundamentally similar to the previous step in the FEM process. This step utilizes the same

geometry and meshing pattern that was developed for the linear version of the three-dimensional modeling. The main difference between the two methods is the solver that was used for the analysis. To conduct this analysis the FEMAP solver "Advanced Nonlinear Static" was used, and this essentially allowed for a time-dependent load to be applied to the model.

In order to simulate the cold expansion process, a ramp function was generated that applied a surface pressure up to a maximum value following a linear trend over the period of 0.5 s and then decreased the surface pressure back to a zero value by the end of the 1.0 s. The maximum value with this generated function is meant to correspond to the point in the cold expansion process when the thickest part of the mandrel is inside the fastener hole, providing the expansion, and the minimum value corresponds to the mandrel being removed from the fastener hole. A plot of the generated function can be seen in Figure 3.6. It can be seen that the maximum value is a unit, this is because the function acts as a scaling factor that is applied to the defined load. The actual maximum surface pressure would be the same value defined in the linear static model.

While defining the analysis for the Nonlinear solver, the number of steps that the solver should run was required to be defined along with the number of iterations for each step. In FEMAP, the number of defined steps is what time increment the solver is divided into, for simplicity of future analysis of results the number of steps was defined as ten. In doing so, each step corresponded to 0.10 s leading to results that show the progression of load development similar to what is shown in Figure 3.6.

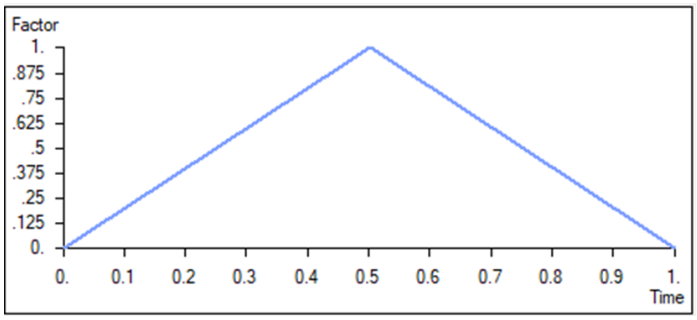

Figure 3.6 Ramp function generated in FEMAP to modify the surface pressure applied as a function of time.

A defined number of iterations is related to the solver's ability to converge to an adequate result at each individual step. The solver reiterates the calculations until convergence is reached or until the number of defined iterations is exceeded. If the number of iterations is exceeded, then the solver will alert that a solution could not be found leading to troubleshooting for the proposed routine. For this analysis, the number of iterations for each step was limited to ten for a faster solution time. It is important to note that no step during the solution exceeded the limit for iterations. This simulation was conducted to watch the development of compressive stress and strain percentage around the fastener hole as the mandrel is pulled through, simulating the cold expansion process. The results of this simulation will be discussed in Chapter 4.

3.4. Strain Mapping of Cold Expansion

The development of residual strain during the cold expansion process can be physically seen by mapping the development of deformation during the process. This strain mapping can be accomplished by using two-dimensional Digital Image Correlation (DIC). DIC is an optical method used to determine the displacements of a loaded structure (Blanc & Aubert, 2019) by examining the displacement of "speckles" that are deposited onto the surface of the testing specimen. For this research, the DIC software

was VIC-2D version-6, produced by Correlated Solutions (Irmo, SC), and the speckling pattern was applied with paint spray as will be discussed further.

3.4.1. Speckle Analysis

Producing a correct speckling pattern is important for accurate calculation of the displacement field by the DIC software. If the speckling pattern is too sparsely applied, then the DIC software will be using a small number of points to make calculations for the displacement of a significant area. Conversely, if the applied speckling pattern is too dense, the software cannot differentiate between the individual speckles, leading to inaccurate results. Because of the importance of applying an appropriate speckling pattern, an investigation into speckle application was conducted.

An appropriate speckle pattern was determined by changing two variables that played a role in the density of the pattern, spray distance and number of layers. The spray distance is the distance measured between the surface to be speckled and the nozzle of the spray paint canister, RUST-OLEUM® (Vernon Hills, IL) Painters Touch® 2X Ultracover® Paint plus Primer black flat. Spraying from a farther distance from the specimen prevented larger paint particles from landing on the specimen, which would cause larger speckles, affecting the accuracy of the strain mapping. However, as the spray distance increased it became more difficult to control where the speckling was being applied, leading to some areas of the surface remaining uncovered.

The other variable, number of layers, is simply how many passes were made with the spray paint to ensure adequate coverage of the surface. It is important to note that a new layer was applied to the surface of a specimen after microscope observation and after the previous layer had dried to avoid the merging of wet speckles. A variety of spray distance and layer combinations were applied to the experimental specimens by providing quick

spritzes of paint, allowing the paint to dry, and then repeating the cycle until a favorable number of layers was reached. Examples of a variety of speckle patterns that were applied can be seen in Figure 3.7, these images were taken using a UHM350-11 digital HDMI microscope manufactured by United Scope LLC (Irvine, CA).

(a)

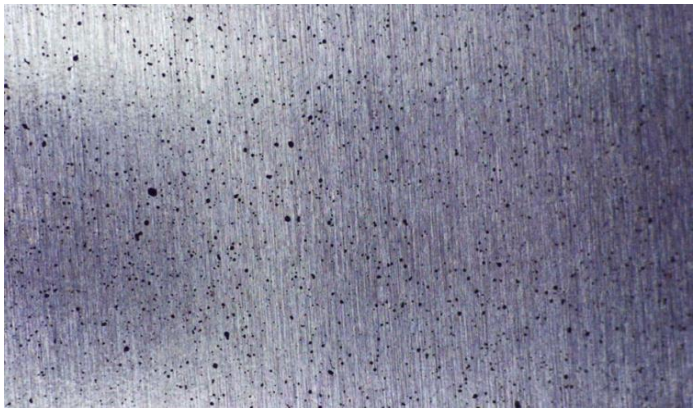

(b)

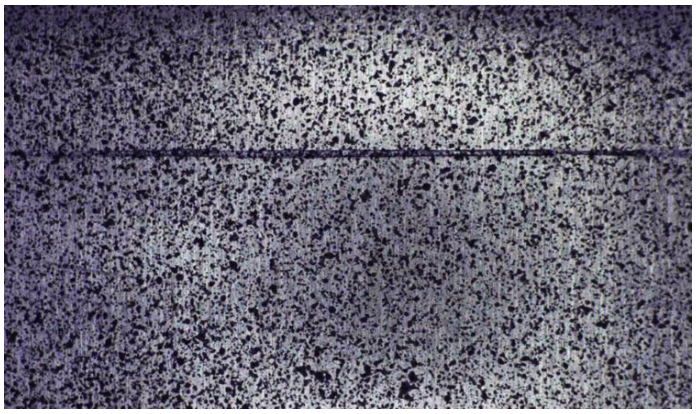

(c)

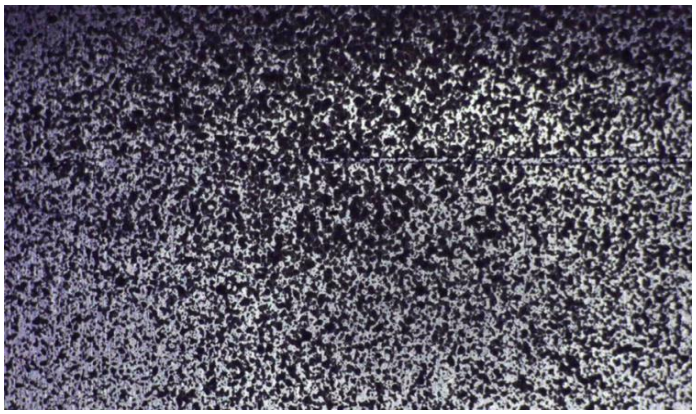

Figure 3.7 Variety of speckle patterns from speckle analysis (a) Spray Distance = 0.9144 m, Layers = 1 (b) Spray Distance = 0.6096 m, Layers = 3 (c) Spray Distance = 0.3048 m, Layers = 2

To determine if a speckle pattern was appropriate for mapping strain development during the cold expansion process, a simple correlation was run in the VIC-2D software. Two sequential images were taken of each speckle pattern with no loading applied, this entails that the strain calculations done by VIC-2D should have a value of zero and show no strain present throughout the pattern, and it was determined there should be a standard deviation of less than 0.1% for the strain calculations meaning there is not a wide variety in reported values. Besides the appropriate speckle pattern density, two variables can be manipulated to affect the software's calculations as well, subset and step size.

Subset size is the size of the division that the software cuts the image into for calculations to find the average strain for the mapped point. If the subset size is too large, a large number of displacement fields will be used to average the strain in a specific point, increasing accuracy, but reducing resolution. If the subset size is too small, then there may not be enough speckles for an accurate calculation of local strain. An example of a subset size reference applied to the image can be seen in Figure 3.8.

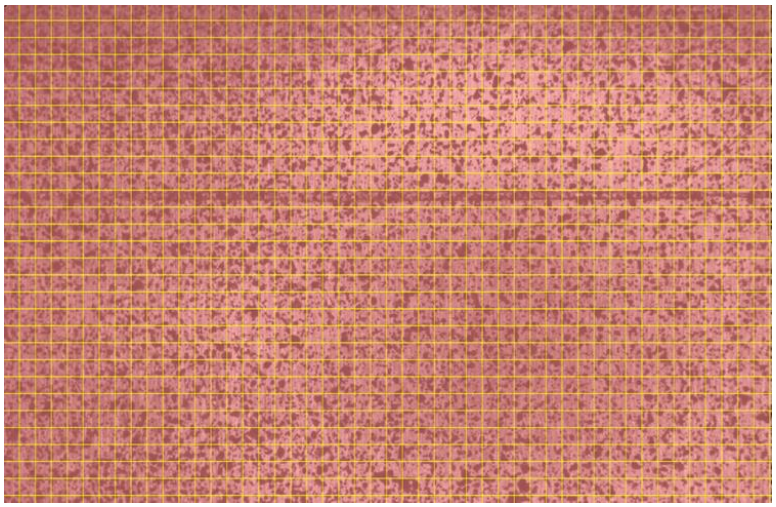

Figure 3.8 Example of a subset division of a speckle pattern produced by VIC-2D 6 software.

The step size is simply how many pixels the software jumps to calculate the strain. For example, if the step size is five, the software will calculate the strains every five pixels. The result of strain between calculated points is interpolated by the software in the strain map. If the step size is too large then the calculation of the strain is not an accurate representation of what is physically occurring, and if it is too low, then the computational time will increase. The smaller the subset and step size the higher the computation time necessary to solve the mapped surface. After an appropriate speckle density and pattern was determined, the DIC analysis can be performed, with the results presented in Chapter 4.

3.4.2. Strain Mapping of Cold Expansion Application

The images for DIC were taken while the cold expansion was applied to the specimens. The cold expansion of the fastener hole was applied similarly as diagramed in Figure 1.3, with the 0.216 mm (0.0085 in.) thick split-sleeve being slid onto the lubricated tapered mandrel with a maximum thickness of 0.748 cm (0.2945 in). The mandrel was connected to the Fatigue Technology Incorporated (FTI) (Seattle, WA) HP-10 Hand Puller which would be pulling the mandrel through the split-sleeve and fastener hole.

The mandrel-split-sleeve combination was inserted into the fastener hole, so that the mandrel was entering through the side of the experimental specimen that had the speckling pattern applied to it. The specimen was held stable by a vice with the digital microscope being placed on the speckled side, the experimental apparatus can be seen in Figure 3.9. A 3.175 cm ($1\frac{1}{4}$ in.) socket wrench, seen in Figure 3.10, was used to turn a nut on the back of the hand puller which in turn pulled the mandrel through the

split-sleeve and hole. A 1.11 cm ($\frac{7}{16}$ in.) wrench, Figure 3.10, was used to stabilize the mandrel in the hand puller while the cold expansion was being applied.

After each half-turn of the 3.175 cm socket was completed, an image was taken with the digital microscope to observe strain development during the application of the cold expansion. This process was repeated until the mandrel was fully through the fastener hole. The images taken during the cold expansion process were uploaded to the VIC-2D software with appropriate step size and subset size applied to map the strain development. The strain mapping can be seen in Chapter 4.

Figure 3.9 Experimental apparatus of speckled sample and UHM350-11 digital microscope to map strain development during the cold expansion process.

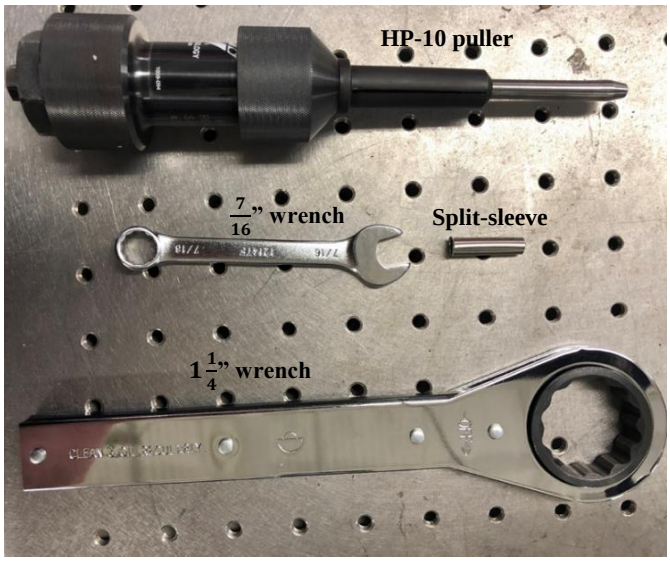

Figure 3.10 Equipment used for split-sleeve cold expansion of fastener hole.

3.5. Fatigue Testing of Experimental Specimens

The process for fatigue testing will be discussed below. There were two trials ran for fatigue testing to examine the life of the specimen with a fastener hole. A controlled trial and an experimental trial. The setup for both trials will be detailed below. The fatigue experiments were completed by using a 100 kN MTS (Eden Prairie, MN) frame tester with MTS 647 Hydraulic Wedge Grip, and an MTS 661.21A-02 load cell. An MTS 407 Controller was used to input and read the loading parameters for the experiment.

To facilitate crack initiation, a thin sharp razor blade was used to apply a small cut into the fastener hole wall, Figure 3.11(a). As can be seen in Figure 3.11(b) the UHM-350 11 digital microscope was placed on the side of the specimen where the cut had been applied. The specimen was then subjected to fatigue cyclic loading until a small crack was detected at the edge of the cut in the fastener hole wall. After the detection of crack-initiation, cycles were run at 1,000 cycles at a time, periodically stopping throughout the complete life of the experimental specimen.

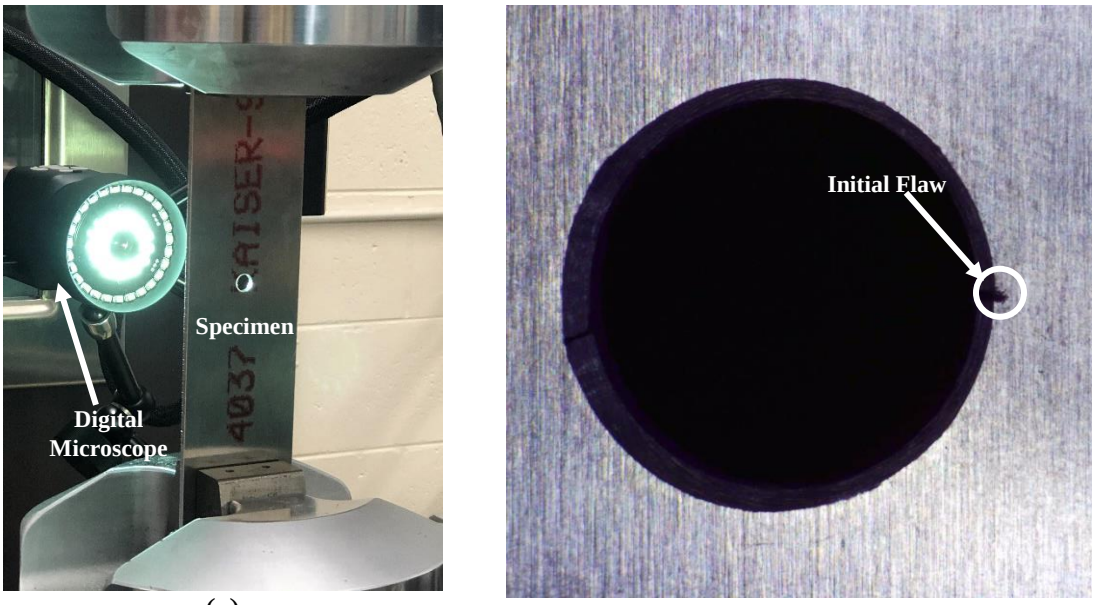

(a) (b)

Figure 3.11 (a) Digital microscope set up to track crack growth during fatigue cycling (b) Initial cut made with a razor blade to control crack initiation.

After every 1,000 cycles, an image was taken with the digital microscope so that the growth of the crack could be tracked inside the Kopa Capture Software that was compatible with the microscope. It is worth noting that as the crack grew and failure was imminent, the interval between images was reduced to ensure crack growth could be monitored. As the main question to be answered in this research work is related to the benefit of not previously cracked cold-worked holes will have in fatigue, the second sample had the cold expansion process applied upon the detection of the crack. After the application of cold expansion, the process of monitoring growth of the crack was followed until the failure of the specimen. After the failure of both specimens, the crack growth process was recorded and can be seen as reported in Chapter 4.

For fatigue testing, certain variables have to be defined. The MTS 407 Controller required three inputs of variables related to fatigue. The first was the setpoint, essentially from the average stress defined in Chapter 1, which acts as the initial loading that the

MTS machine will apply to the specimen when activated. The second variable was span, from the amplitude stress defined in Chapter 1, is the range of tensile loading that the MTS machine will apply during the testing. Finally, the frequency behaves in the same manner as discussed previously in Chapter 1.

For the crack initiation process, several checks were performed to find amplitude stress and mean stress that would initiate a crack in a reasonable time. For this phase, the amplitude stress was set at 42.9 MPa (6.22 ksi) and the mean stress was 50.26 MPa (7.29 ksi) leading to a maximum stress of 93.2 MPa (13.51 ksi). These values were chosen so that the specimens would be under a third of their yield stress for crack initiation. After crack initiation, a newly defined force combination was used throughout the life cycle of the specimen, with an amplitude stress of 88.25 MPa (12.8 ksi) and mean stress of 107.9 MPa (15.64 ksi) leading to a maximum stress of 196 MPa (28.44 ksi).

The testing variables used throughout the initiation of the micro-cracks for both specimens can be seen in Table 3.4, including initial variables that were used at the beginning of experimentation. It is worth mentioning that while the frequency of the cycling was for the majority of testing held to 1 Hz, it was reduced at certain stages of the experimentation to provide better monitoring of the crack opening and closing during testing.

Crack length measurements taken by the Kopa Capture software during the growth of the crack for the fatigue life cycle of both specimens can be seen in Chapter 4. Images taken by the digital microscope showcasing the crack growth during the life of both specimens can also be found in Chapter 4.

Table 3.4

Variables used during fatigue testing for crack initiation cycles and crack propagation cycles.

Condition	**Variable**	**Specimen 1**	**Specimen 2**
Crack Initiation	σ_a, MPa (ksi)	42.9 (6.22)	88.25 (12.80)
	σ_m, MPa (ksi)	50.26 (7.29)	107.9 (15.64)
	R	0.079	0.100
Crack Propagation	σ_a, MPa (ksi)	88.25 (12.80)	88.25 (12.80)
	σ_m, MPa (ksi)	107.9 (15.64)	107.9 (15.64)
	R	0.100	0.100

4. Results

Using the previously defined experimental methods, each stage of the research was completed throughout this thesis. Appropriate values and figures found during the procedures of the experiment will be reported in the following chapter. A deeper discussion of the results and how they relate to the overall objective of this research will be conducted in Chapter 5. The results presented in this section will include the analytical calculation describing the cold expansion process, FEM simulation results of the cold expansion process, DIC of the cold expansion process, and the fatigue experiments of specimens.

The results of the analytical calculations will exhibit the predictive development of the stress region during and after the expansion process. In addition, the numerical values that led to the corresponding dimensions of the specimens will be described. Analysis results of the three different FEM simulations of the cold expansion process will be reported below as well. These results will consist of contours of nodal displacement, strain, and stress developments throughout the expansion process. The maximum values that are achieved during the expansion process will also be shown.

The results of the speckle analysis for DIC will be presented to show what the speckle density and pattern was used for the strain mapping during the cold expansion of the fastener hole. The strain contours produced by the VIC-2D software during the cold expansion process will also be shown in this chapter. Results of the fatigue crack growth during testing will be shown later in this chapter as well. Pictures of the crack growth at different stages of the propagation with a tabulated growth through the full lifecycle of the specimens will be seen as well.

4.1. Analytical Calculations for Cold Expansion

The development of the residual stress region during the application of cold expansion can be solved using the Elastic-Plastic theory equations shown in Section 2.3. Also, the analytical calculations using the Elastic-Plastic Theory affected the dimensioning of the Al 2024-T3 specimens used for fatigue life experiments. The dimensioning of the specimen was determined iteratively by examining what combination of system external diameter and hole diameter allowed for the radial residual compressive stress to be zeroed at the specimen external boundary.

With this iterative calculation combined with the available mandrel diameter and split-sleeve thickness, the cold expansion percentage to be applied to the fastener hole could be found. Using Equation 6, the cold expansion applied for this experiment was calculated to be 4.95%. This will be the percent of strain when the thickest part of the mandrel is in the hole with the sleeve, and it will be used as a gauge for the FEM analysis. This value is appropriate because it was desired to have a cold expansion degree similar to what is conducted in the industry, which is between 4 and 5 percent.

Another important value defined with the analytical calculations is the radial displacement that will be caused by the mandrel and sleeve, U_m. This value will be used as the deformation applied in the two-dimensional FEM analysis and also as a calibration for the surface pressure applied in the three-dimensional calculations. Using Equation 7, the radial displacement caused by the mandrel and the sleeve was found to be 0.189 mm (0.007438 in). Also from Equation 7, the plastic zone radius, *c*, found by iteratively solving for U_m was found to be 13.7 mm (0.5395 in).

With the values of the previously defined *a*, *b*, and *c* and the conditions required for reverse yielding being met, the reverse yield radius could be found through iteratively

solving Equation 14 by plugging in the relevant values. It was found that the reverse yielding radius was 4.468 mm (0.1759 in). All relevant values found with Equations 16 through 18 can be used to plot the development of the residual stress regions measured from the edge of the hole. The tangential and radial residual stress regions as created by using the Elastic-Plastic Theory equations can be seen in Figure 4.1.

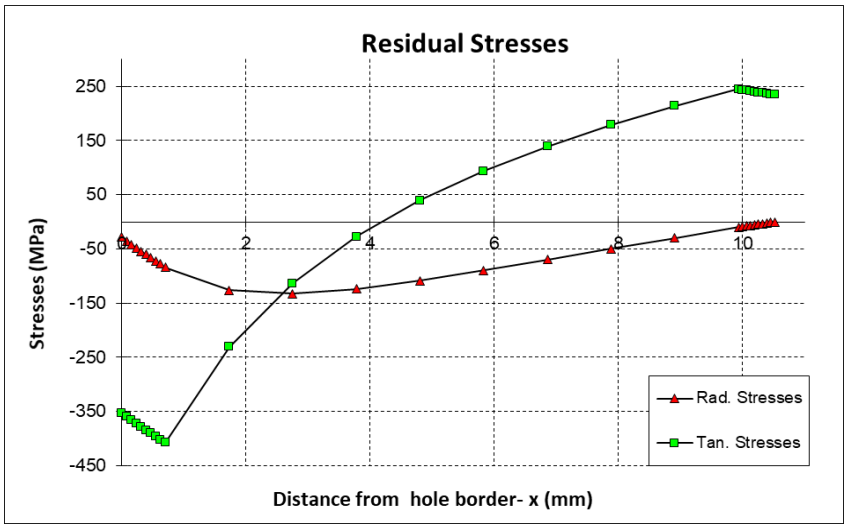

Figure 4.1 Tangential and radial residual stress region development from the hole edge.

It can be seen in Figure 4.1, that the residual stress regions for both radial and tangential feature a compressive nature as evidenced by the negative stress values. The tangential residual stresses, which are the most important aspects of the residual stress regions show a minimum compressive stress region near the edge of the hole while gradually becoming more positive the farther from the hole edge. It can be seen in Figure 4.1 that the residual tangential stress region features a reasonable compressive zone up to 4.0 mm (0.16 in) from the hole border. It is rather evident that the residual stress region leads to an improved fatigue life as the large tangential compressive region must be

overcome and does not stop inhibiting the growth of a fatigue crack until the crack has grown enough to bypass the compressive zone.

The radial residual stress region development away from the hole edge shown in Figure 4.1 exhibits compressive stress behavior throughout the region. It was important to allow for the full development of the radial residual stress region and a smooth return to zero stress by having adequate specimen material available. If the width of the specimen was not adequate, then the residual stress region would be impacted, and this could reduce the benefit of cold expansion. Thus, the dimensioning of the specimens was affected by the analytical calculation of the residual stress development.

To provide more detail of the stress development effect on the specimen dimensions, as can be seen in Figure 4.1, the radial residual stress region did not zero out until the distance from the hole was slightly greater than 10.5 mm (0.4 in). This means the required width of the specimen needed to be greater than 21 mm (0.8 in), plus the hole diameter, when considering that the expansion would affect both directions away from the hole. Meaning that the width of the manufactured specimens, 57.15 mm (2.25 in), as found in Table 3.3 is more than adequate to allow for the full development of the residual stress region.

4.2. Finite Element Modeling of Cold Expansion

The main goal of the FEM simulation of the cold expansion process was to simulate the expected radial displacement caused by the mandrel and split-sleeve, and compare the FEM residual stress results of an elastic-plastic bi-linear model with the ones obtained by the application of plasticity theory for an elastic perfectly plastic material. Theoretically, simulating this radial displacement should lead to the correct cold expansion degree being applied to the fastener hole. To reiterate from Section 4.1, the applied radial displacement

by the mandrel and the split-sleeve was analytically calculated to be 0.189 mm (0.007438 in) and the cold expansion degree was 4.95%. The FEM simulations were run as described in Chapter 3 and the results will be reported below. The results will be in the form of contour plots generated by FEMAP that will aid in the understanding of the development of the residual stress regions. Both quantitative and qualitative observations made on the stress contours will also be presented in the following sections.

4.2.1. Two-Dimensional Linear Static Modeling

As discussed in Section 3.3.1, the purpose of the two-dimensional linear static modeling was to verify that if applying the radial displacement to the nodes around the edge of the hole would yield the corresponding degree of cold expansion from the calculations. Only the full application of the mandrel and split-sleeve were considered for this simulation process. The contour of the major principal strain developed by the radial displacement can be seen in Figure 4.2. It was assumed that the major principal strain displayed by FEMAP would correspond to the degree of cold expansion applied to the hole. This assumption was made for all FEM simulations of the cold expansion process as well as the DIC analysis following in the next section. The major principal strain referred to as cold expansion degree from here on, calculation provided by FEMAP, would be multiplied by 100 to convert to percent strain to correspond to the cold expansion percentage.

As can be seen in Figure 4.2, the cold expansion degree contour shows a maximum degree near the hole edge, shown in the bright red color on the contour. The cold expansion degree then shows a decrease in value the farther away from the hole edge the simulated elements are, as evidenced by the dark blue color and the pink-colored areas at the farthest points from the hole edge. This development is to as expected because the

farther away from the edge of the hole the less effect that the mandrel being pulled through the hole would have. The pink and dark blue regions that developed farther from the edge of the hole represent the elastically strained regions, with strain below 0.5%, which will ultimately force the plastically deformed areas back to their original locations creating the residual compressive stress region.

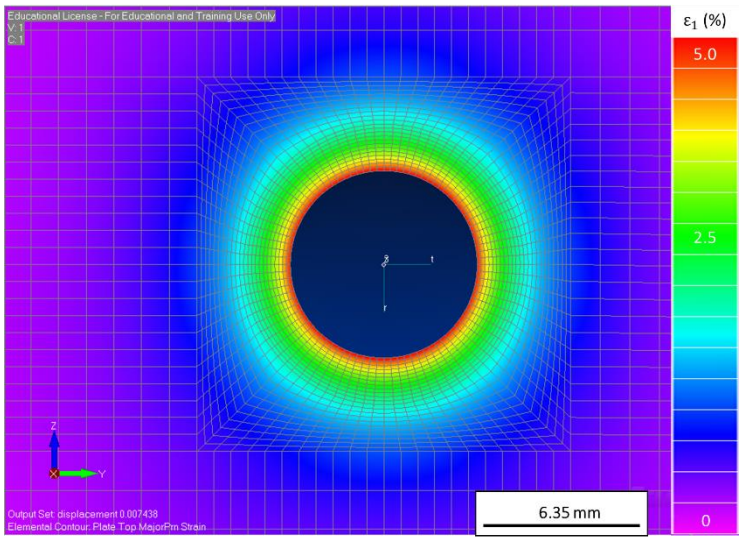

Figure 4.2 Major Principal strain development around the hole after mandrel and split-sleeve radial expansion of 0.189 mm applied, simulating the cold expansion degree.

After applying the calculated radial displacement, it was expected that the calculated cold expansion degree would be reached in the two-dimensional simulation. However, this was not the case as the cold expansion degree reached through the simulation was slightly greater than the expected, 4.95%, at 5.09%. An investigation was conducted by running another simulation to determine what applied radial displacement would lead to the correct expansion degree. Multiple simulations were run with a new radial displacement applied to the hole border nodes until the appropriate expansion degree was found. The corresponding displacement was found to be 0.184 mm (0.007229 in) and the

contour developed with this new displacement can be seen in Figure 4.3. It can be seen that the contour develops in the same manner with the maximum expansion degree found at the hole edge. It is worth mentioning that the analytically calculated radial displacements would be the desired value for the future simulations and not the newly found value.

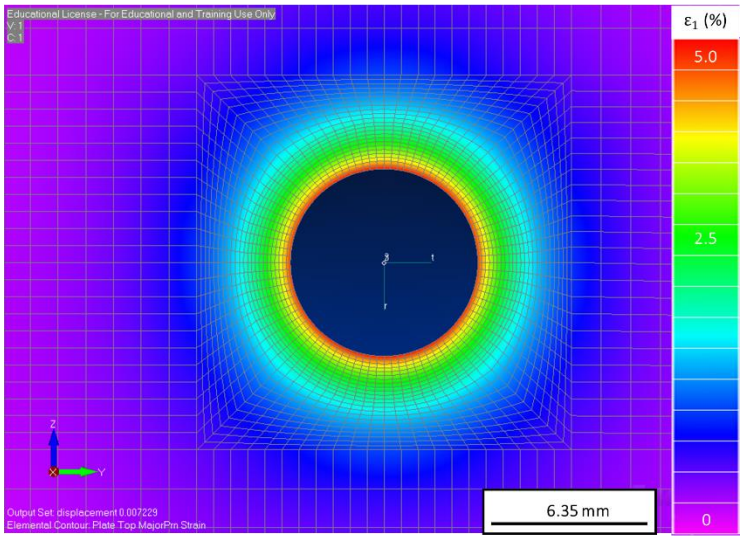

Figure 4.3 Major Principal Strain development around the hole after mandrel and split-sleeve radial expansion of 0.184 mm applied, simulating the cold expansion degree.

4.2.2. Three-Dimensional Linear Static Modeling

The three-dimensional linear elastic static model was conducted with the main purpose of determining a surface pressure value, that when applied to the inner wall of the hole would radially displace the hole to an equivalent value of mandrel and split-sleeve displacement. This was accomplished iteratively by running multiple simulations and varying the surface pressure applied. Similar to the two-dimensional liner analysis, only the point where the major diameter of the mandrel and the split-sleeve are in the hole were considered for this analysis. This surface pressure was determined to be

244 MPa (35.411 ksi). Applying this pressure and running the linear static analysis yielded contours that were applicable to understanding the behavior of the specimen at the cold expansion degree.

The first produced contour was is the displacement of the nodes around the hole edge and the regions around the hole. This is simply the radial displacement caused by the applied surface pressure, as it can be seen in Figure 4.4. The maximum value seen in the bright red around the hole was calculated to be 0.189 mm (0.00743 inches), which was the expected value caused by the mandrel and split-sleeve showing that the surface pressure was appropriate for simulation. It should be worth noting that the contour developed smaller radial displacements even farther away from the hole edge. This shows that the surface pressure applied to the inner hole wall affects the entire surrounding area during the cold expansion.

The second contour developed by the calculations conducted in the three-dimensional analysis was the cold expansion degree. Similar to the contour developed in the two-dimensional analysis the maximum value was found at the edge of the hole, with the expansion degree decreasing the farther from the hole. The maximum expansion degree of this contour at the edge of the hole was found to be 5.01%. This was rather close to the predicted value from the analytical calculations. The contour for cold expansion degree can be seen in Figure 4.5.

The third relevant contour developed by the three-dimensional linear analysis is the von Mises stress contour. The von Mises stresses were used as the gauge for stress development because when defining Al 2024-T3 as a bi-linear material in FEMAP, it required the von Mises failure criteria to aid the nonlinearity. The von Mises stress contour can be seen in Figure 4.6.

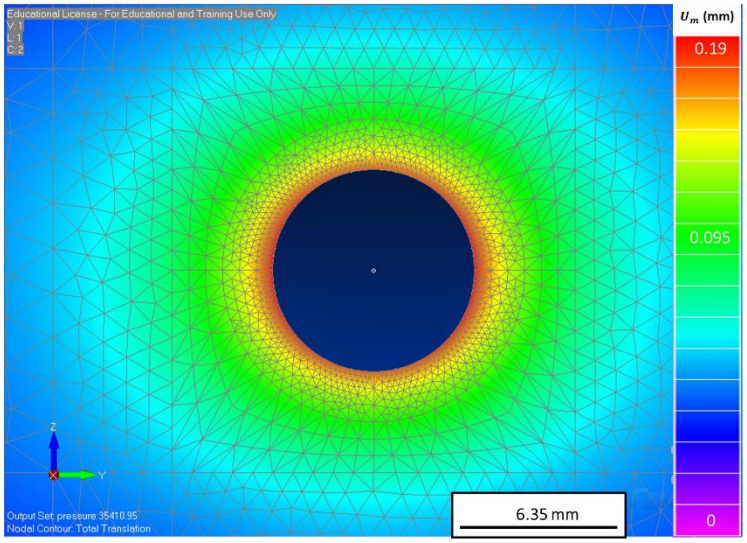

Figure 4.4 Radial displacement contour caused by surface pressure applied to simulate cold expansion.

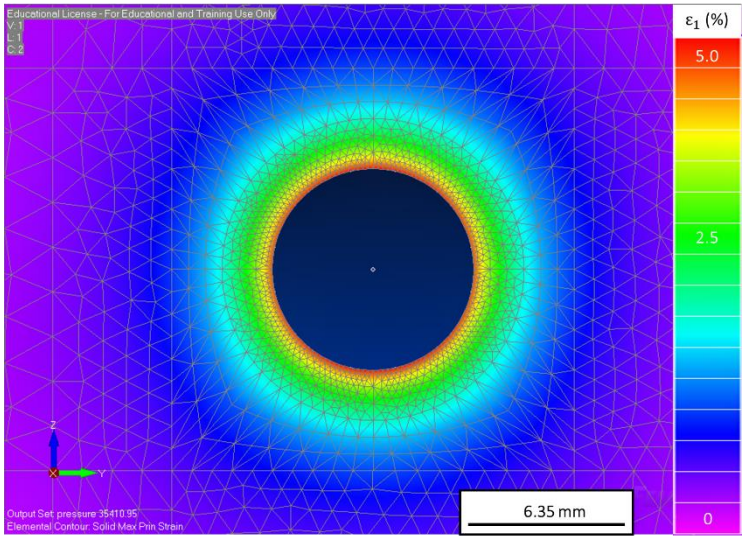

Figure 4.5 Cold expansion degree contour caused by surface pressure applied to simulate cold expansion.

Like the previous two contours shown before the von Mises stress contour displays the same transition from a maximum stress value near the edge of the hole to lower stress values at the farther regions shown in Figure 4.6. The maximum von Mises stress at the border of the hole was valued at near 438 MPa (63.5 ksi). Recalling that this is a

linear-elastic analysis and the yield stress of Al 2024-T3 is 324 MPa (47.0 ksi), this contour shows that the region near the hole border experiences stress values that lead to the material to yield and begin to plastically deform. This contour confirms the previously explained process that occurs during the cold expansion.

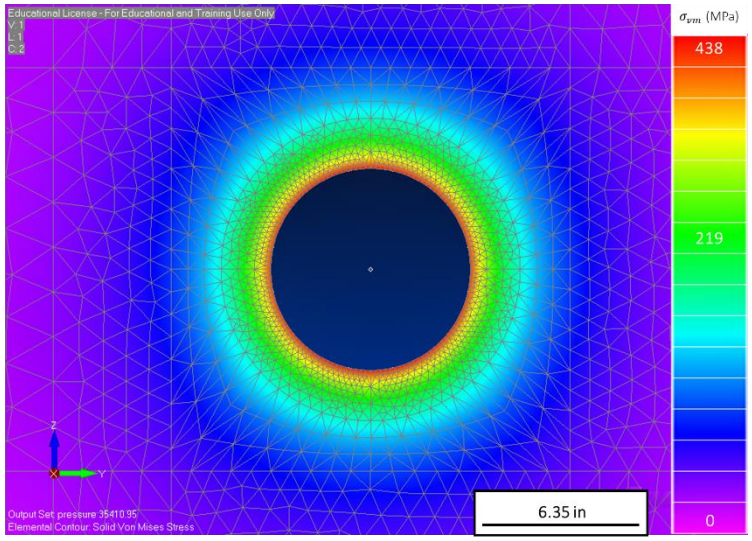

Figure 4.6 The von Mises Stress contour caused by surface pressure applied to simulate cold expansion.

4.2.3. Three-Dimensional Nonlinear Static Modeling

The purpose of the three-dimensional nonlinear static modeling as discussed in Section 3.3.3 was to model the full cold expansion process with the mandrel being fully pulled through the hole. Because of the nature of the advanced nonlinear solver, the surface pressure that was applied in the previous modeling method did not provide the radial displacement that was used to mimic the cold expansion. A more applicable surface pressure was determined iteratively like the two-dimensional linear analysis previously. This surface pressure was determined to be 233 MPa (33.837 ksi).

Like the previous two modeling methods, the development of values of interest was presented in the form of contours. These values include the radial displacement, the cold expansion degree, and the von Mises stresses. Another value that was examined specifically for this modeling method was the development of plastic strain, which was calculated by the advanced nonlinear solver. The contour development for each value of interest can be seen in the series of figures below. Important steps of the mandrel beginning to be pulled through corresponding to time 0.1 s, the thickest part of the mandrel being in the hole corresponding to time 0.5 s, and the mandrel being removed from the hole corresponding to time 1.0 s. The contours developments at other points of time for each of the values of interest can be found in Appendix B.

The radial expansion during the cold expansion process as the mandrel is drawn through the split-sleeve and hole can be seen at three different stages in Figure 4.7. As can be seen in each image the radial displacement around the hole becomes more and more prominent as the mandrel is drawn through the hole, cumulating in the maximum radial displacement at time 0.5 s which is equivalent to the thickest part of the mandrel being in the hole. This maximum value was found to be the calculated 0.189 mm from the analytical calculations, showing that the appropriate radial expansion has been applied. As expected when the mandrel has been removed at time 1.0 s, the radial displacement returns to near the original starting radius.

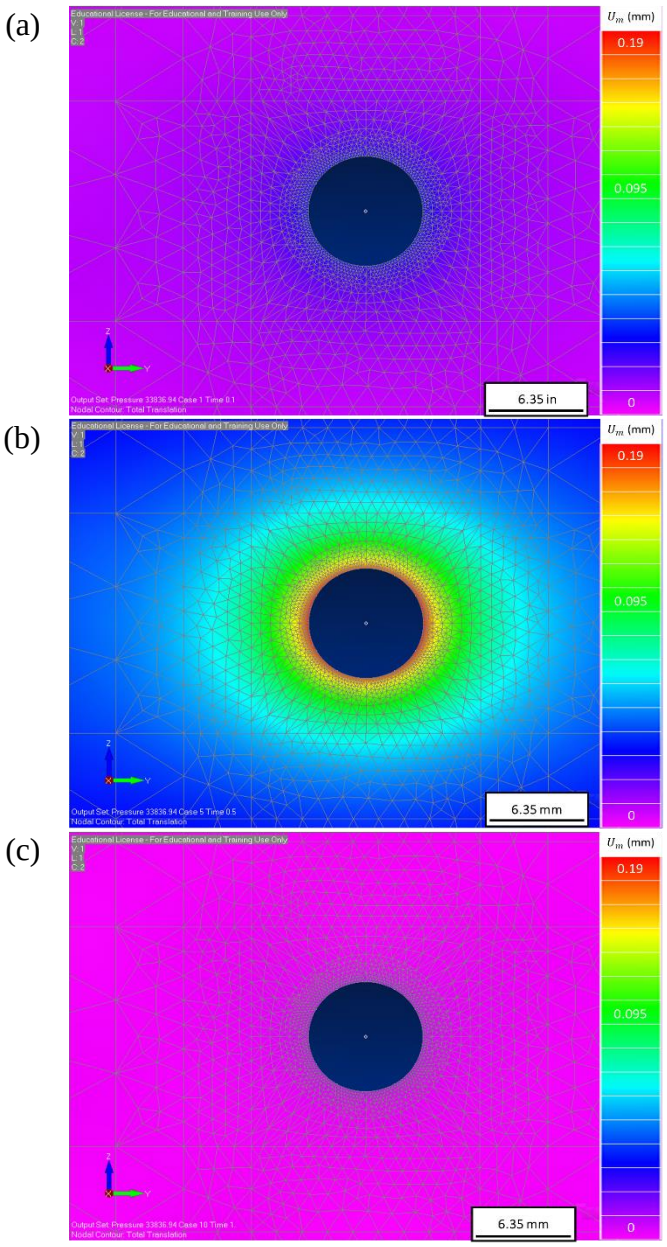

Figure 4.7 Radial displacement development around hole during cold expansion process (a) Corresponding time: 0.1s (b) Corresponding time: 0.5s (c) Corresponding time: 1.0s.

The development of the cold expansion degree in the form of contours can be seen in Figure 4.8 at the three different stages. As expected the degree of cold expansion increases as the mandrel is drawn through the hole. The maximum cold expansion degree at time 0.5 s for this analysis method was found to be 5.07% which is again slightly

higher than the expected 4.95% calculated analytically. The cold expansion degree then proceeds to decrease as the mandrel is fully drawn through the hole.

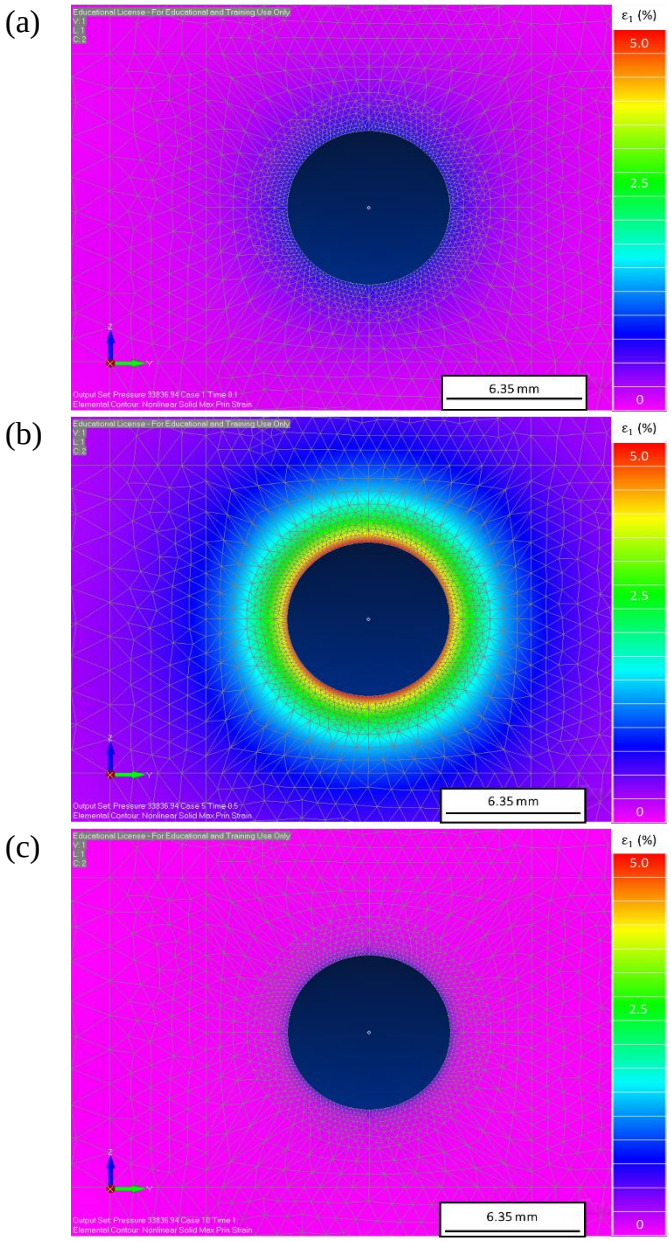

Figure 4.8 Cold expansion degree development around hole during cold expansion process (a) Corresponding time: 0.1s (b) Corresponding time: 0.5s (c) Corresponding time: 1.0s.

As mentioned earlier, FEMAP provides a contour detailing the plastic strain that has been developed while the analysis was being conducted. This plastic strain development throughout the expansion process can be seen in Figure 4.9. This development shows an important thing with regards to the cold expansion. Recall, that the area around the hole is to be plastically deformed during the cold expansion process while the region farther from the hole edge is only elastically deformed. It can be seen in Figure 4.9(b) which corresponds to the point where the thickest part of the mandrel will be drawn through the hole, meaning that the simulation shows that when the mandrel is at the hole it begins having plastic deformation. It is also worth noting as seen in Figure 4.9(c) that even after the mandrel has been removed from the hole there is still a lasting impact from the mandrel in regards to the plastic strain. The plastic strain contour shows that during this simulation the expansion process appears to been applied as expected.

The contours developed for the von Mises stress levels during the application also provide a prediction for the development of the plastic strain seen in Figure 4.9. As can be seen in the series of contours shown in Figure 4.10 at the time corresponding to the maximum pressure application, Figure 4.10(b), and the mandrel being in the hole the von Mises stress shows a maximum value of 345 MPa (50.136 ksi) around the hole edge. Recall, the limit stress, found in Chapter 3.1, of the material is 324 MPa, meaning that the experienced applied stress around the hole does in fact exceed this limit stress. This would mean that when the thickest part of the mandrel is at the hole interface the area around the hole will have plastically deformed and the material was hardened following the inputted elastic-plastic curve. This supports what was found in Figure 4.9 with the development of the plastic strain.

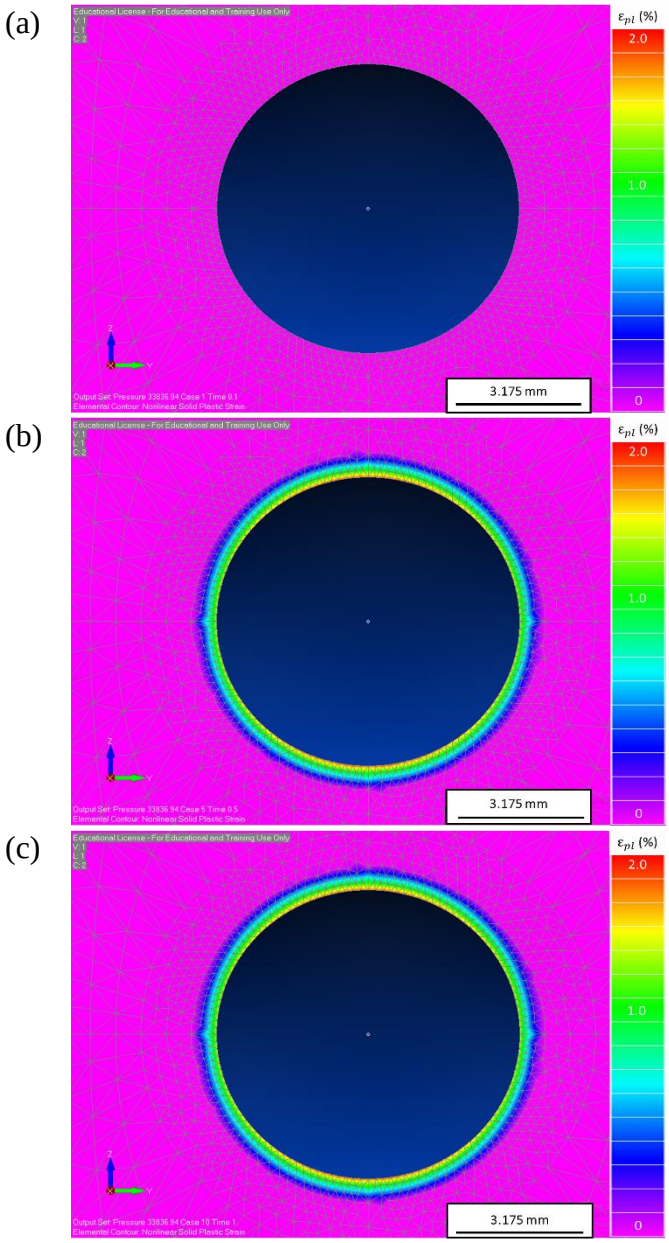

Figure 4.9 Plastic strain development around hole during cold expansion process (a) Corresponding time: 0.1s (b) Corresponding time: 0.5s (c) Corresponding time: 1.0s.

After the mandrel has been fully drawn through and removed which corresponds to time 1.0 s in the FEM simulation, residual stress is present in the contour Figure 4.10(c). In order to visualize more, this image has been reproduced in Figure 4.11 with a more appropriate stress value to saturate the contour. This presence of residual stress in the contour shows that the simulation of the expansion provides the development of the stress

which will act as the counter to improve fatigue life. The radial development of the residual stress region follows a similar trend that was seen throughout all contours during this simulation. The closer to the hole edge the higher the residual stress value is, with the value of stress decreasing the farther from the hole, for instance in the elastic area.

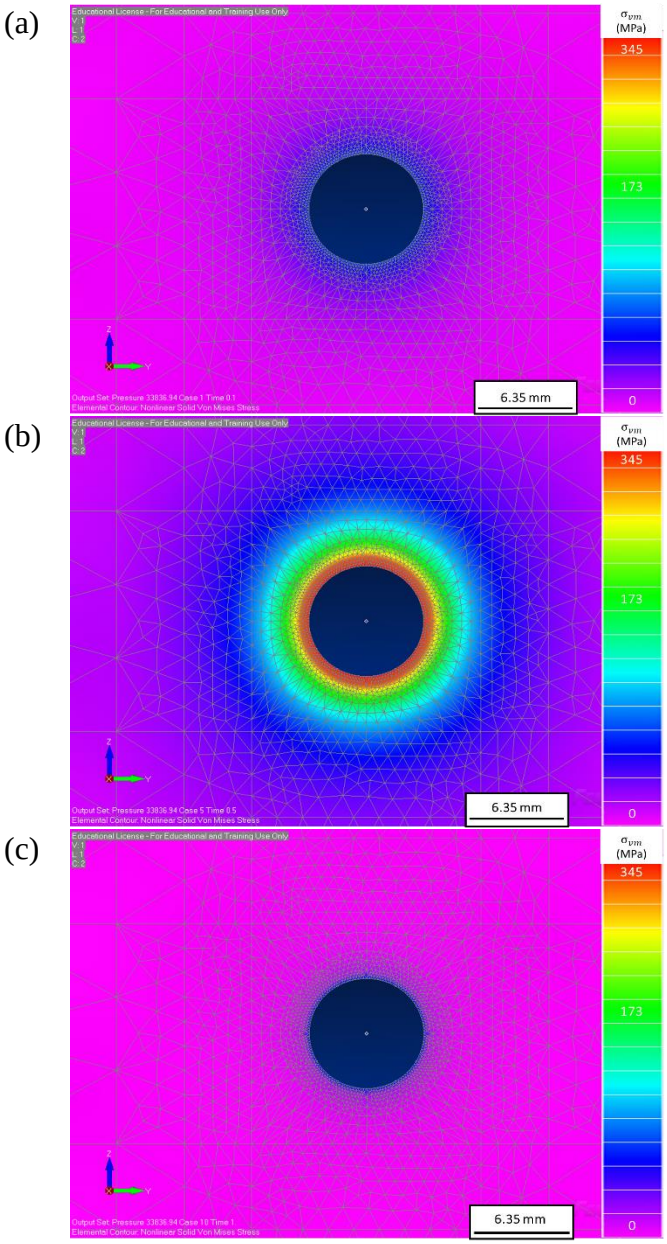

Figure 4.10 Von Mises stress development around hole during cold expansion process (a) Corresponding time: 0.1s (b) Corresponding time: 0.5s (c) Corresponding time: 1.0s.

The maximum value of the stresses around the hole at 1.0 s as highlighted in Figure 4.11 was calculated to be approximately 85 MPa (12.273 ksi). It is worth noting that FEMAP reports the von Mises stresses as a relative tensile stress value, or a positive value when in reality this would be measured as a compressive stress or a negative value. Comparing this maximum residual stress region around the hole to the analytical calculations in Section 4.1 the values are significantly lower. But the presence of the residual stress does show that the FEMAP simulation is exercising the expected principles of the cold expansion process.

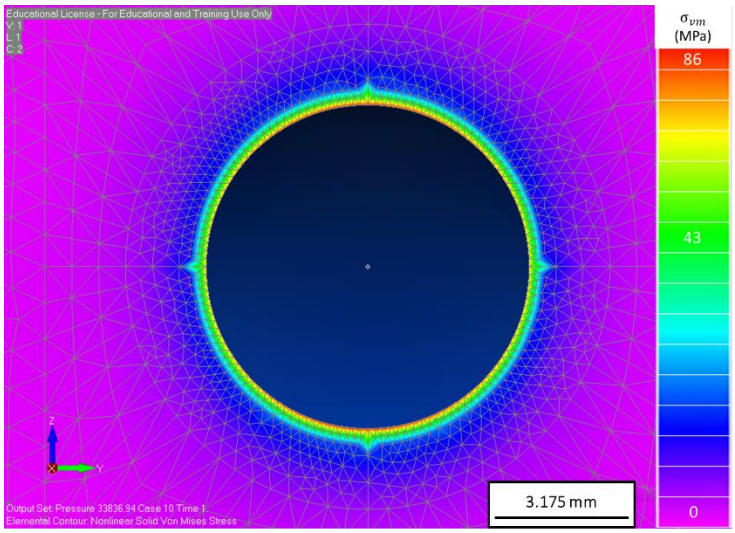

Figure 4.11 Saturated contour at time step 1.0s showing the residual von Mises stress region after mandrel has been removed.

To provide a different way to visualize the development of the various values of interest throughout the cold expansion application, the maximum values at each step for the radial displacement and expansion degree were taken from the contours and plotted below in Figure 4.12. It can be seen that both the maximum radial displacement, Figure 4.12(a), and the cold expansion degree, Figure 4.12(b), develop similarly to as the surface

pressure was applied shown in Figure 3.6, with the values ramping up to the 0.5-time step and then back down as the time step moved towards 1.0 s.

(a)

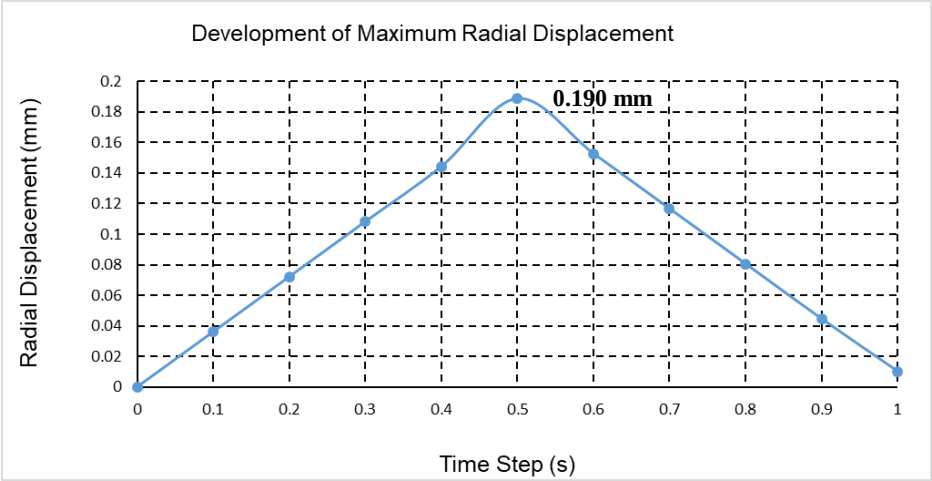

(b)

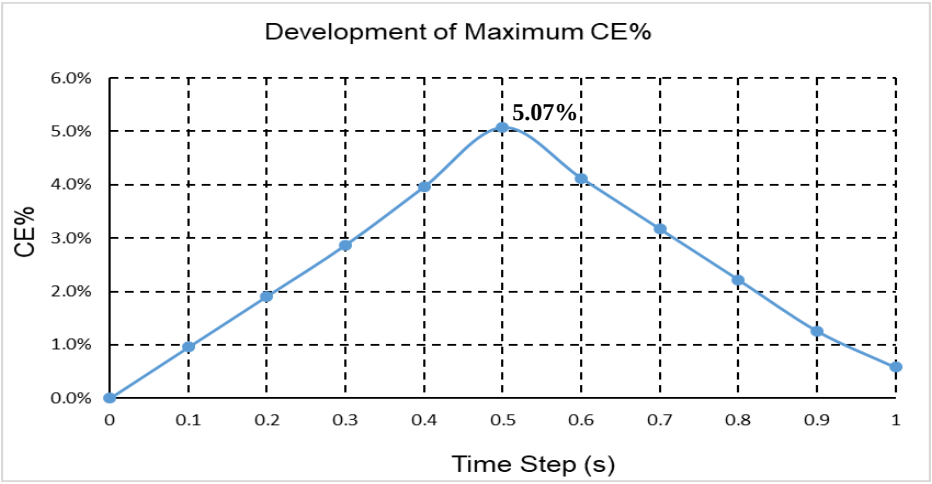

Figure 4.12 Development of the maximum (a) radial displacement and (b) cold expansion degree as cold expansion is applied.

The maximum value of the von Mises stresses when plotted as the time increases, Figure 4.13(a) also follows the similar ramp trend until 1.0 s is reached. This increase between 0.9 s and 1.0 s highlights the development of the residual stress region that was highlighted in Figure 4.11. Also in Figure 4.13(a), the limit stress being exceeded during the cold expansion can be reiterated. A secondary line was added to the von Mises stress

graph corresponding to the limit stress, and it can be seen that yield stress is slightly exceeded at 0.4 s before fully exceeding the limit stress at the expected 0.5 s time step.

(a)

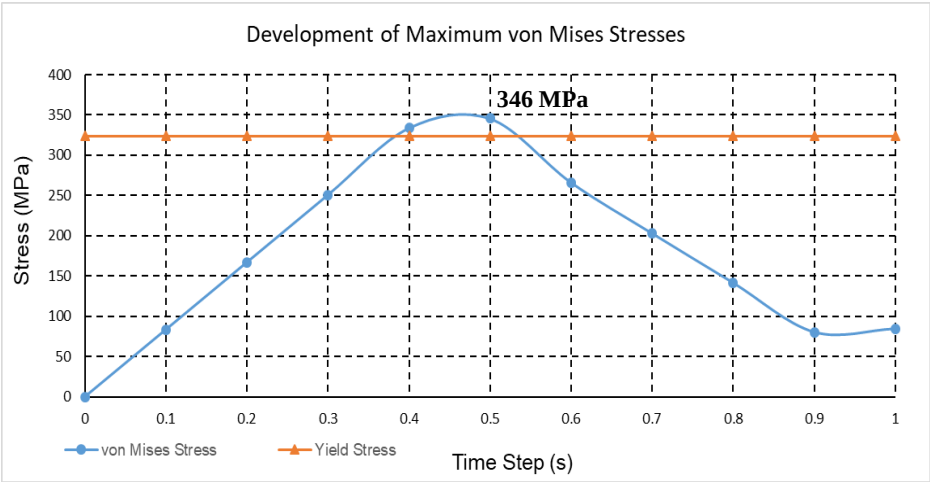

(b)

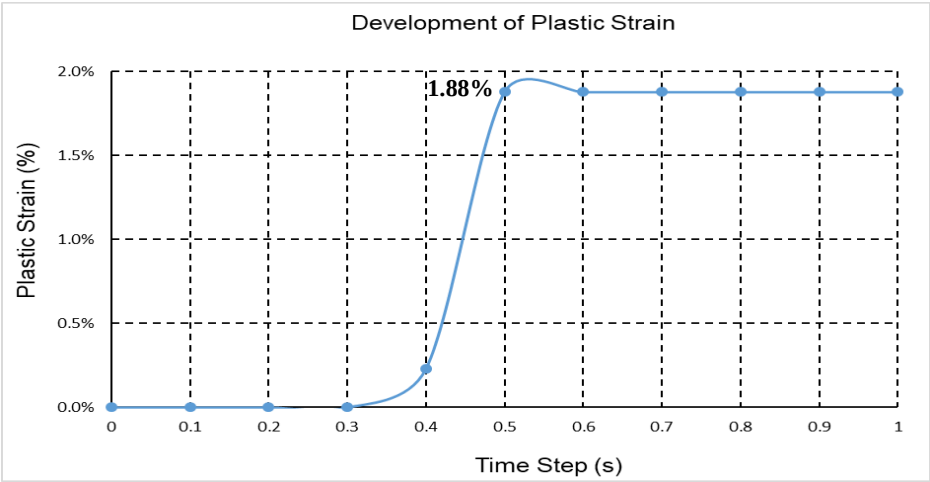

Figure 4.13 Development of the maximum (a) von Mises stresses and (b) plastic strain as cold expansion is applied.

The maximum value of the plastic strain contours can be seen in Figure 4.13(b). As discussed in the contour development, there was no plastic strain shown until the limit stress is exceeded. This also corresponds with the von Mises stress development in Figure 4.13(a), as the plastic strain begins to develop at the same time that the limit stress is exceeded at 0.4 s. It is also shown in the later points of Figure 4.13(b), that once the

plastic strain is developed it remains constant, showing that the expansion applied has a lasting impact on the areas around the hole.

While the values reported throughout the nonlinear static analysis may have been lower than expected based on the analytical calculations, the simulation provided valuable information about what occurs during the expansion process. For instance, the simulation showed that the drawing of the mandrel through the fastener hole exceeded the limit stress of the material for an area around the hole. As a consequence, these specific areas plastically deform yielding as evident by the creation of plastic strain regions around the hole edge. It was also seen by the simulation, that the areas farther away from the hole edge experienced reduced values of all contours shown. This fundamentally makes sense as the effect of the mandrel would be minimized in these regions.

This development of plastic regions was expected when analyzing the Elastic-Plastic Theory in Section 2.3. The plastic region development also allows for the observation of the residual stress region once the mandrel has been completely drawn through the hole. This residual stress region creation, although minimal compared to the analytical calculations, shows that the simulation of the cold expansion did affect the material around the hole in the expected fashion. Therefore, the simulation method while simplified does provide good qualitative results.

4.3. Strain Mapping of Cold Expansion Using DIC

DIC was used in the attempt to map the strain development during cold expansion. Also, this method has the potential of keeping the information of residual strain after the mandrel has been removed. The mapping of the strain by the VIC-2D DIC software will be discussed in the following section. First, recall from Chapter 3 that before the cold

expansion effect could be mapped, an appropriate speckle density and pattern had to be determined. A summary of the results from this speckle analysis will be provided in the following section.

4.3.1. Speckle Analysis

As mentioned in Chapter 3.4 the speckling pattern and density were manipulated with variables of distance and number of layers. The distance was varied so that the nozzle of the paint spray was 0.3048 m away from the specimen surface to 0.9144 m away from the specimen. The number of layers was varied from one to three layers. Multiple sets of combinations of these variables were sprayed onto the Al 2024-T3 samples, with an example of different speckle patterns being seen in Figure 3.7.

DIC analysis was conducted on images of these speckle patterns to determine which pattern provided appropriate results for strain mapping. Recall that the subset size and step size were manipulated to allow for a low standard deviation, 0.1% and low average percent strain, aiming for 0%, when computed between two different reference images of the same specimen. Finding an adequate subset size was done in a two-step process. The first step was done by using the subset size automatically calculated by VIC-2D for the provided image. The DIC was conducted and the corresponding standard deviation and average principal strain were tabulated, this table can be seen in Appendix C. The lowest automatic step size was then lowered until it provided a standard deviation of around 0.1% and then applied to each speckle pattern image.

This process was repeated until the subset size could not go smaller without providing a standard deviation greater than 0.1% and the average percent strain was tabulated. The appropriate step size to be applied for the DIC analysis was determined to be three as it provided an accurate representation of the strain for a subset size without requiring much

interpolation by the software. The appropriate speckle density and pattern as well as subset size and step size can be seen in Table 4.1 below.

Table 4.1

Appropriate speckle pattern requirements and DIC analysis parameters.

Spray Distance, m (ft.)	# of Layers	Subset Size (px)	Step Size (px)
0.6096 (2)	3	35 & 37	3

The strain mapping produced for a specimen with the parameters from Table 4.1 applied can be seen in Figure 4.14.

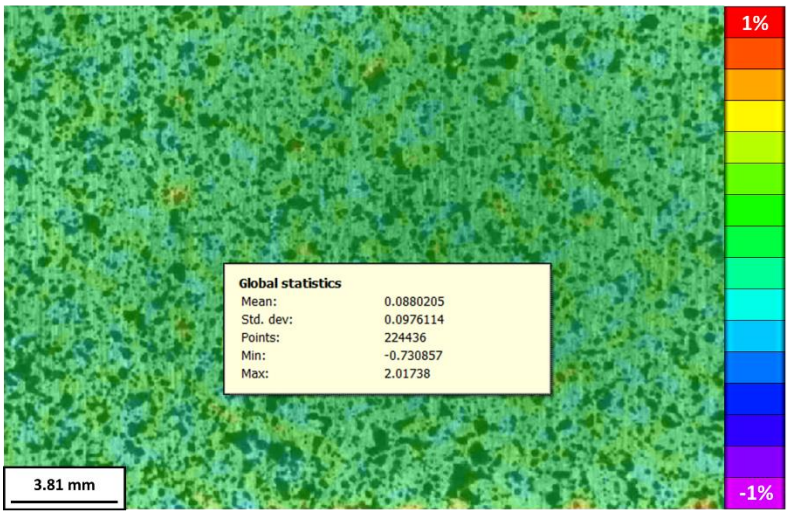

Figure 4.14 Strain mapping of the speckled sample with all appropriate parameters applied.

As can be seen, the standard deviation of the appropriate speckle pattern is within the required 0.1% value for an acceptable strain mapping. It can also be seen that the average percent strain calculated in this mapping was 0.088%. Recall that there was no strain or displacements applied to the specimen so a strain percentage of 0% should have been reported; however, this value was deemed to be reasonably low and acceptable within the

expected uncertainties in the DIC method. It is worth noting that the strain calculated by the VIC-2D software was listed as e_2 Lagrange strain. The e_2 Lagrange strain represents the minor principal strain and most typically represents the most negative value for the in-plane strain. This negative strain value corresponds with compressive strain values and was deemed a good representation for the development of cold expansion degree during the mandrel drawing.

4.3.2. Strain Mapping of Cold Expansion Application

The development of the cold expansion degree while the process was applied was monitored with DIC. The parameters that were deemed appropriate for both the speckling of the surface and the analysis parameters in the VIC-2D were used for this strain mapping. As mentioned in Section 3.4, the cold expansion with tapered mandrel and split-sleeve assembly was applied to the clamped specimen as seen in Figure 3.10. An image of the specimen surface was taken after every half-turn of the wrench to monitor the development of the expansion degree.

It is worth noting that the speckling was only applied to the immediate area around the hole as this was the appropriate area of interest. Also, due to symmetry, only one side of the specimen was photographed during the expansion application, this was done to provide a better resolution for the VIC-2D software. After the images were taken and the appropriate analysis parameters applied the DIC analysis was run for all images taken during the expansion process. During the analysis, it was determined that there were two strain contours produced that relay important information in regards to the cold expansion application. These two strain contours correspond to the point in time when the thickest part of the mandrel is in the hole, and after the mandrel has been removed. A variety of manipulations have been applied to these two contours for qualitative analysis. Note, the

contours have been saturated around the yield strain of Al 2024-T3 to provide clear images of the developments, once it was determined that the current speckling and image resolution was not adequate to provide an accurate gradient for the strain map.

One important information that can be obtained from the DIC analysis is the direction vectors of the principal strain. These directional vectors show the major direction of change of strain calculated by the VIC-2D software and can be seen in Figure 4.15(a) and (b) for the maximum mandrel and removed mandrel respectively. As can be seen, the directional vectors, represented as black arrows, follow a circular path around the hole edge, with a majority of the arrows pointing in the tangential directions. The fact that many of the arrows tend towards the tangential direction and can be considered the major direction hints at the importance of the residual tangential stress region on the fatigue performance of cold expanded fastener holes.

It can also be seen in Figure 4.15(a) and (b) that the length of the major directional vectors decreases between the contour for maximum mandrel thickness and the removal of mandrel. This change in vector length along with the decrease in the magnitude of total strain around the hole edge showcase that the mandrel removal contour showcases the residual plastic strain produced by the cold expansion, whereas the first contour, shown in Figure 4.15(a), showcases a combination of elastic and plastic strain, with the difference in the depth of the two contours being related to the elastic strain. This is synonymous with the unloading of a material that has yielded and subsequently plastically deformed.

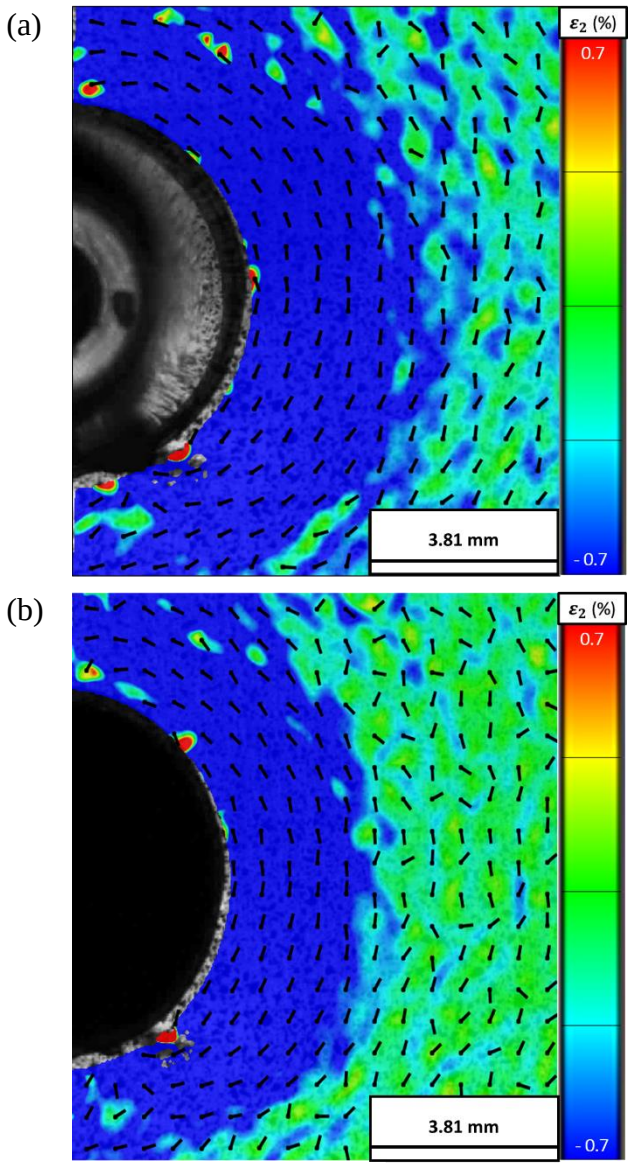

Figure 4.15 DIC e_2 Langrage strain contours for cold expansion process with major direction vectors applied for (a) mandrel in hole and (b) post cold expansion.

The second important information that can be obtained from the DIC maps is the radial displacement vectors that can be superimposed to the corresponding contours. As can be seen in Figure 4.16(a), the contour corresponding to the thickest part of the mandrel being drawn through the hole, the radial displacements feature a higher magnitude as compared to when the mandrel is removed. This experimentally shows that

when the mandrel is drawn through the hole it displaces the material around the hole with the most displacement occurring at the hole edge as evident by the longer vectors.

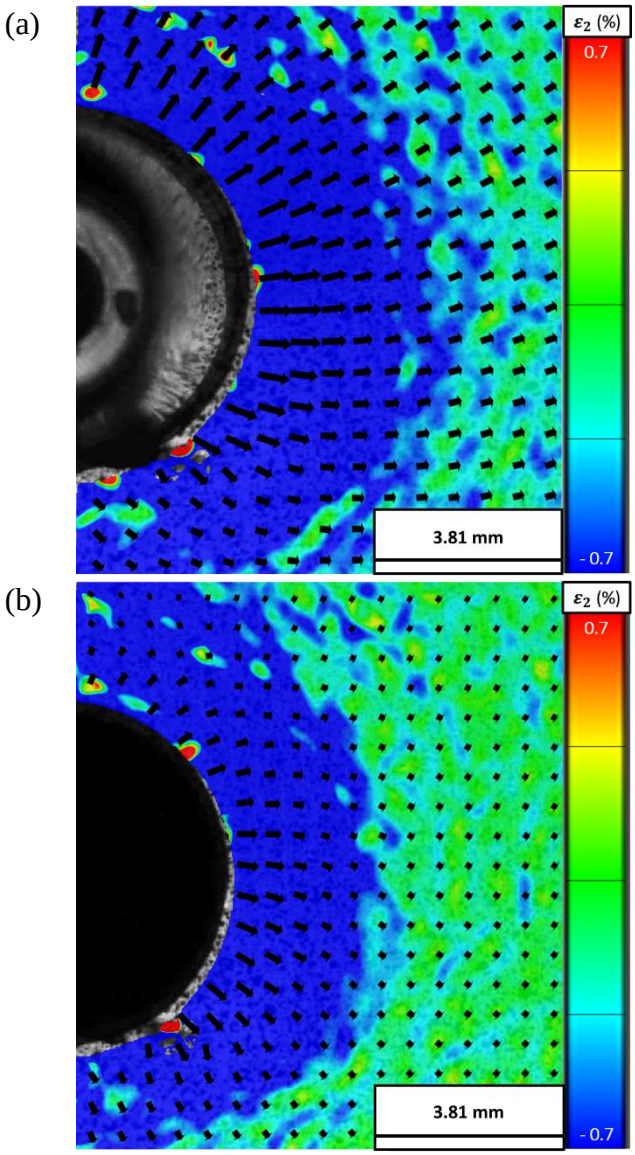

Figure 4.16 Saturated e_2 Langrage strain contours for cold expansion process with displacement vectors applied for (a) mandrel in hole and (b) post cold expansion.

The contour corresponding to the removal of the mandrel, Figure 4.16(b) also shows the radial displacement. Note that the VIC-2D software makes its strain calculations by comparing it to a reference image with no boundary conditions applied, meaning that the

direction of the arrows are showing that the speckles tracked by the software are radially displaced compared to the reference image. However, the decrease in the magnitude of the vectors compared to the vectors shown in Figure 4.16(a) showcase that the material around the hole had some return to its starting material, this is synonymous with the "snapping back" caused by the elastic region. The negative direction tendencies of the displacement vectors shown in Figure 4.16(b) is most likely caused by the specimen having a slight vertical displacement. Because the specimen was only clamped at the bottom during these experiments the mandrel being pulled through would cause a vertical displacement upwards, and once the mandrel was removed the specimen would return to its original vertical equilibrium.

The contours produced by the VIC-2D software produced nonuniform contours which were expected after analyzing the cold expansion in FEMAP. The speckle size, although deemed acceptable for a surface that was not experiencing any displacements or strains, was possibly too large to allow for accurate calculations. However, saturating the strain contours around the limit strain for Al 2024-T3 allowed for a more uniform development to occur and provide useful imagery on the effect that the cold expansion had on the material when the mandrel is at the hole and especially when the mandrel has been removed.

The distribution of red areas (local high strain) located in the images Figure 4.15(b) and Figure 4.16(b) correspond in their majority to errors prevenient from inadequate speckling regions. In addition, it is expected that close to the sleeve split region, some variation in the predicted strain should occur. As the sleeve is opened in the cold work process, it created this concentration which may have impacted the development of strain around the entirety of the hole edge. Houghton (2010) recommends that the location of

the split be in the least critical direction of crack growth because the opening of the split causes asymmetrical development of residual stresses meaning lower hoop stresses around the split. What this means is that because oftentimes the crack will grow perpendicular to the loading direction, the split in the sleeve should be oriented parallel with the loading direction. For the application of cold expansion for specimen two during the fatigue testing, assurance was made so that the split was oriented in the 12 o'clock direction to alleviate this issue.

4.4. Fatigue Testing

As mentioned in Section 3.5, after a small cut in the edge of the hole was made with a razor blade, fatigue cycles were conducted until the point of crack initiation. The loading parameters that were used for the crack initiation of both specimens can be seen in Table 3.4. It is worth mentioning that for specimen one, which was the as-drilled specimen, the crack initiation load parameters were increased to the higher values as seen in Table 3.4 so the number of cycles that were required for crack initiation, presented in Table 4.2 will represent this load change. For the specimen that underwent cold expansion, the crack initiation loading was the higher value as seen in Table 3.4.

As can be seen in Table 4.2, it required fewer amount of cycles to initiate the crack at the higher loading parameter than it did at the lower, which fundamentally makes sense as higher stresses are applied. Measurements of the crack length were taken every 1,000 cycles in the Kopa Capture software. The measurements taken for specimen one can be seen in Table 4.3. It is worth noting that the crack length measured was the straight-line length from the edge of the hole to the tip of the crack, so whatever turns and directions were not factored into the crack length.

Table 4.2

Number of cycles required for crack initiation of each specimen at the designated loading.

Specimen	Loading	Cycles	Cycles to Initiation
Specimen 1	$\sigma_{Max} = 93.2\ MPa$	60,260	66,278
	$\sigma_{Max} = 196\ MPa$	6,018	
Specimen 2	$\sigma_{Max} = 196\ MPa$	2,061	2,061

Table 4.3

Cycle count and crack length for the as-drilled specimen.

Cycle Number	Crack Length (mm)	Cycle Number	Crack Length (mm)
0	0.254	**3,800**	3.531
800	0.813	**4,800**	5.359
1,800	1.524	**5,800**	8.585
2,800	2.337	**6,256**	10.73

As can be seen, the as-drilled specimen sustained 6,256 cycles until failure with an initial crack of 0.254 mm, and a critical crack length of 10.73 mm. This means that once the crack was discovered the specimen had slightly over 6,000 cycles of life before failure at the given loading parameters. Images taken during the growth of the crack can be seen in Figure 4.17, with the tip of the crack being highlighted on each image. It was seen during the fatigue testing near the end of the life of the specimen that the opening and closing of the crack was more prominent. The ease of opening and closing at the later stages of fatigue life can be seen by the greater change in crack length.

(a)

(b)

(c)

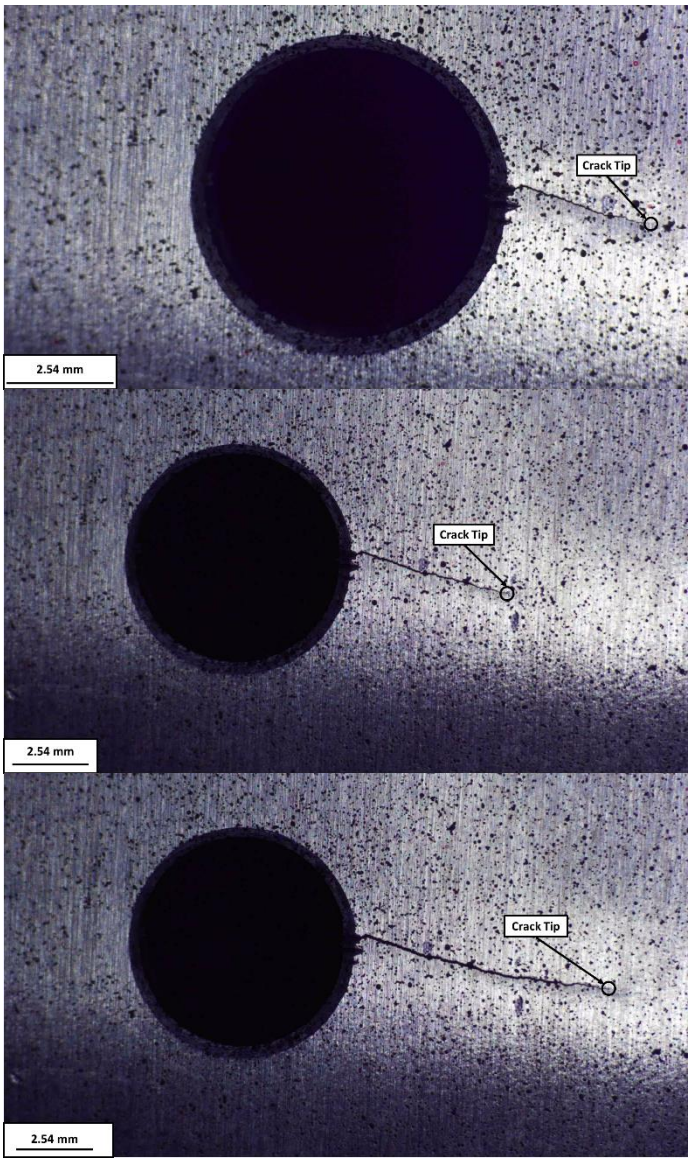

Figure 4.17 Crack growth for specimen one during fatigue testing with crack tip location noted (a) 3,800 cycles (b) 4,800 cycles (c) 5,800 cycles.

For specimen two, after it was noted that the crack had initiated the cold expansion was applied to the hole. This is the main point of this work. It is to show the real effect of cold expansion in pre-cracked components. The specimen was then fatigued with measurements taken in the same manner and results can be seen in Table 4.4. It can be seen that specimen two, which received the cold expansion after the presence of a crack was noted, had an extended fatigue life with a final cycle count to failure of 70,983, from

an initial crack of 0.254 mm. This time to failure was 11.3 times greater than that of the as-drilled specimen. Not only was the life cycle of the specimen longer but the rate at which the crack grew while inside the compressive zone was much reduced.

Table 4.4

Cycle count and crack length for the cold expanded hole.

Cycle Number	**Crack Length (mm)**	**Cycle Number**	**Crack Length (mm)**	**Cycle Number**	**Crack Length (mm)**	**Cycle Number**	**Crack Length (mm)**
0	0.254	**14,000**	0.965	**31,500**	1.194	**52,500**	1.702
500	0.305	**15,000**	0.991	**32,500**	1.194	**53,500**	1.702
1,000	0.356	**16,000**	0.991	**33,500**	1.219	**54,500**	1.727
1,500	0.406	**17,000**	1.016	**34,500**	1.219	**55,500**	1.778
2,000	0.406	**18,000**	1.016	**35,500**	1.219	**56,500**	1.829
2,500	0.432	**19,000**	1.016	**36,500**	1.219	**57,500**	2.057
3,000	0.432	**20,000**	1.041	**37,500**	1.245	**58,500**	2.108
3,500	0.457	**21,000**	1.067	**38,500**	1.295	**59,500**	2.235
4,000	0.508	**21,500**	1.092	**39,500**	1.295	**60,500**	2.311
4,500	0.533	**22,000**	1.092	**40,500**	1.346	**61,500**	2.616
5,000	0.584	**22,500**	1.118	**41,500**	1.448	**62,500**	2.896
5,500	0.610	**23,000**	1.143	**42,500**	1.448	**63,500**	3.226
6,000	0.610	**23,500**	1.143	**43,500**	1.473	**64,500**	3.607
6,500	0.610	**24,000**	1.168	**44,500**	1.499	**65,500**	4.013
7,000	0.610	**24,500**	1.168	**45,500**	1.676	**66,500**	4.572
8,000	0.660	**25,500**	1.194	**46,500**	1.676	**67,500**	5.232
9,000	0.686	**26,500**	1.194	**47,500**	1.676	**68,500**	5.994
10,000	0.711	**27,500**	1.194	**48,500**	1.676	**69,500**	6.782
11,000	0.762	**28,500**	1.194	**49,500**	1.676	**70,500**	8.687
12,000	0.889	**29,500**	1.194	**50,500**	1.676	**70,983**	9.533
13,000	0.889	**30,500**	1.194	**51,500**	1.676		

Images of crack growth taken during the fatigue experiment for the specimen undergoing cold expansion can be seen in Figure 4.18. As noted in Table 4.4, for a majority of the life cycles for this specimen there was minute growth which will be evident in the images.

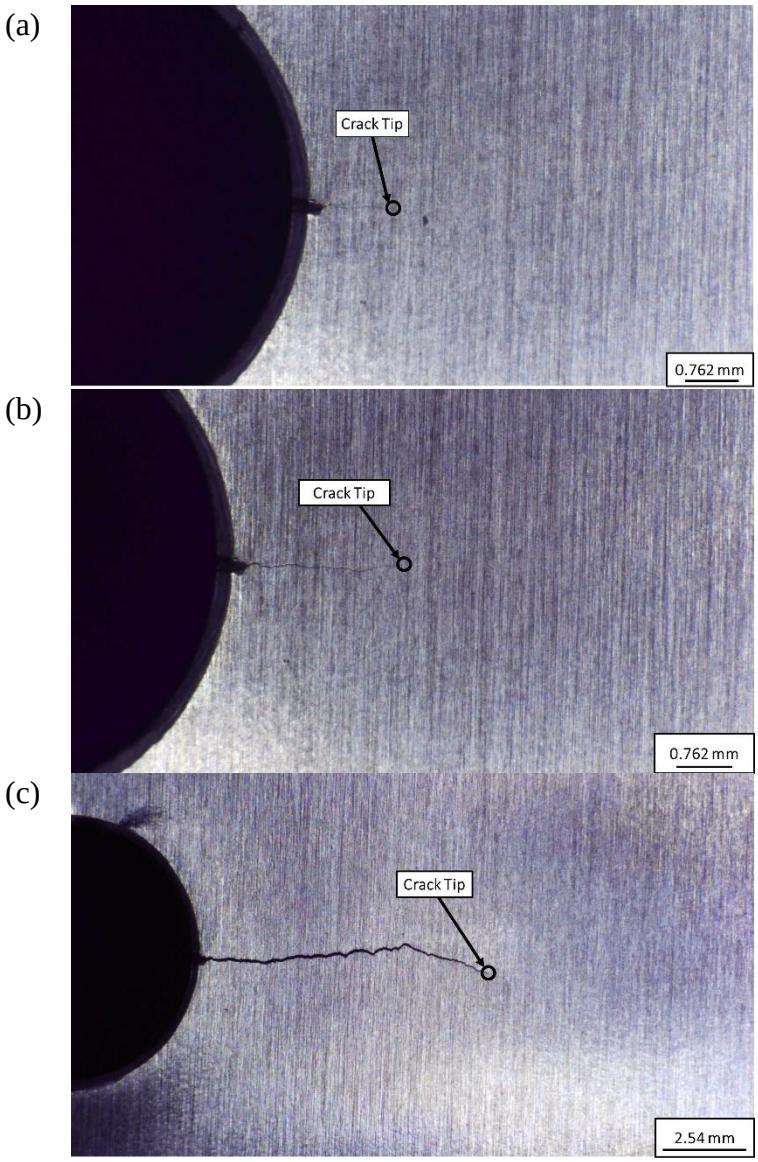

Figure 4.18 Crack growth for specimen two during fatigue testing with crack tip location noted (a) 30,500 cycles (b) 60,500 cycles (c) 70,500 cycles.

Similarly to the as-drilled specimen, the opening and closing of the crack during the later fatigue cycles became more apparent which is evidenced by the faster growth rate. A comparison of the fatigue life for both specimens can be seen in Figure 4.19. When examining Figure 4.19, it becomes apparent the benefit that the cold expansion provided for a specimen even with the presence of a crack at the fastener hole. It can be seen that

the cold expansion increased the fatigue life of the specimen by reducing the growth rate of the crack while in the compressive zone.

Figure 4.19 Crack growth comparison between the as-drilled specimen and cold expanded specimen.

Recall from Section 4.1 that the residual tangential stresses were compressive in nature from the hole edge to 4.0 mm away from the hole edge, as seen in Figure 4.1. This entails that the compressive stresses, in the tangential direction, created by the cold expansion of the hole, are counteracting the tensile loads that are being applied to the hole, thus improving the fatigue performance of the specimen. This compressive stress region can be seen by the rate of crack growth once it surpasses the 4.0 mm limit. As can be seen in both Table 4.4 and Figure 4.19, when the crack length crosses the 4.0 mm boundary and is outside of the compressive zone the curves for open and cold-worked holes have a similar format as the growth rate begins to accelerate. The reason for this is

that the residual compressive stresses no longer are counteracting the applied loads meaning the crack grows faster.

5. Conclusion

The focus of this research was to examine the effect that cold expansion has on the fatigue life of a specimen with a preexisting flaw at a fastener hole. It is well documented that cold expansion applied during the manufacturing stage provides fatigue life benefits when compared to a fastener hole that has not gone under expansion. However, it is unsure what fatigue life benefits the expansion would apply if the hole had a small crack already present. This potential benefit was examined by analyzing the deformation and fatigue testing on Al 2024-T3 specimens with a preexisting small crack, one with applied cold expansion and one without.

For the analytical part, the application of cold expansion to fastener holes was examined using three different methods. The first method was by solving idealized plasticity theory equations from the literature for an elastic perfectly plastic material. The second was a finite element model of cold expansion of a hole by using an internal pressure applied to the inner wall of the hole to simulate the expansion. The third method consisted of mapping the strain developed during the cold expansion process using digital image correlation software. Conclusions gathered throughout this research will be presented below. In addition, recommendations on future research that could build upon the research presented will be discussed.

5.1. Final Remarks

The conclusions that can be drawn based on the different steps of this research can be seen below:

- After conducting analytical calculations using Elastic-Plastic Theory equations, the residual effects caused by the expansion application could be analyzed. It was found that residual stresses in the tangential direction have the most important impact on fatigue

life benefits. These high compressive stress values that make up the tangential stress region would counteract the tensile loading applied to the specimen. For the specimen dimensions and boundary conditions used in this research, it was determined that the compressive stress region would retard crack growth in the region up to 4.0 mm away from the hole edge.

- After simulating the cold expansion process applied to the fastener hole using an advanced nonlinear solver, the qualitative development of plastic deformation and residual plastic regions could be visualized. With an application of surface pressure that produced a maximum cold expansion degree that was 2.39% different than what was calculated analytically, it was found the yield stress of Al 2024-T3 was exceeded when the mandrel was simulated to be in the hole. This exceedance produced the plastic region which would lead to fatigue life benefits. The development of residual stresses at the mandrel removal was also visual.

- Analyzing contours produced by DIC, the plastic region was again able to be visualized during the expansion application. Saturated contours corresponding to the thickest part of the mandrel being in the hole show that a region of compressive stress was more developed than compared to the similar contours corresponding to when the mandrel is removed. This development of the region has a radius corresponding to the predicted plasticity theory equation.

- The DIC contours also support the importance of residual stresses developed in the tangential region are dominant. Applying direction vectors to the contours showcased that the major direction of strain calculated with DIC was in the tangential direction. Changes in the magnitude of the applied vectors show the partial return that the material

around the hole experiences upon mandrel removal. This return further highlights the residual region developed.

- Fatiguing specimens revealed the benefits that cold hole expansion can provide even when there is a presence of cracks. The specimen that did not receive any cold expansion after the detection of a small crack was able to withstand 6,356 cycles of high loading stresses. The specimen that did receive expansion after the small crack was detected was able to withstand 70,983 cycles of the same loading parameters.
- The specimen that underwent cold expansion had a fatigue life improvement of 11.3 times that of the as-drilled specimen. This is a significant improvement on fatigue life even though there was a crack present at the time of application. The effect of the compressive stress region developed by the expansion could be seen as well as noted by the minute changes in crack length as seen in Figure 4.19. The compressive stress region was determined to slow down the crack growth by counteracting the tensile loading applied during the fatigue testing.

5.2. Future Works

This research shows the benefits that cold expansion provides even with the presence of flaws or cracks created by previous fatiguing of aircraft parts. Further investigations can be conducted to explore the benefits of cold expansion application with other conditions that aircraft parts will undergo during their life cycle. A discussion on potential future works will be conducted below as well as improvements that could be made to yield better results.

Lower Loading Parameters

The applied stress during the fatigue cycles was rather high to ensure the specimens in this experiment would present crack propagation within a reasonable time. This

implied that the stresses applied were able to overcome the compressive stress regions developed by the cold expansion as the crack grew. One avenue of future research would be to examine the full effect that the current level of applied cold expansion would have if the applied stresses were lower. Investigations could include tracking the crack growth during the fatigue cycling to determine if the crack growth was diminished even greater or in fact fully halted in its growth as was speculated earlier. The experimental methods for this investigation would be very similar to the methods presented in this research.

Expansion Benefits on Corroded Specimen

Like fatigue, corrosion has an impact on the performance life of aircraft structures. Similar to the basis for the presented research, which looked at the presence of cracks near a fatigued hole after resizing a hole during maintenance, corrosion can be present at or near fastener holes due to the corrosive environment that an aircraft operates in. Potential research on this topic could examine the effect that cold expansion would have on previously corroded structures. Investigations could include examining the effect that the cold expansion will have when applied to a specimen that has had corrosion introduced. Another investigation could be into the effect that cold expansion applied to a fastener hole undergone corrosion and with an initial flaw present. One can investigate the effect of the compressive zone on galvanic corrosion, which could potentially cause new crack formation.

FEA Simulation of Expansion Improvements

Additional FEMAP simulations could be conducted on the cold expansion process changing the application of the cold expansion. Instead of applying the surface pressure, used to simulate the cold expansion, to the entirety of the hole edge at once; applying it variably to simulate the mandrel being drawn through the hole. This could yield a more

accurate simulation of the expansion while allowing the development of residual stresses to be visualized better. Another important contribution would be to include the crack in the FEM cold expansion analysis.

Strain Mapping with DIC Improvements

To obtain the necessary strain map resolution, it is necessary to have a finer speckling and higher magnification images, which will require stitching several images to cover an area of interest. Another possible improvement of the presented research could be monitoring the strain development during the cold expansion in a different method. One method that could be used to monitor strain development is photo elasticity. This method would be a more qualitative method rather than a quantitative method. Rings of color can be observed during and after the expansion method is applied, and similar to contours developed by the DIC software, the ring associated with interferometry analysis would designate the value of strain experienced. This qualitative method would allow for good visualization of the development of the strain.

REFERENCES

Antunes, R. A., & de Oliveira, M. C. L. (2015). Effect of surface treatments on the fatigue life of magnesium and its alloys for biomedical applications.

Bandyopadhyay, R., Mello, A. W., Kapoor, K., Reinhold, M. P., Broderick, T. F., & Sangid, M. D. (2019). On the crack initiation and heterogeneous deformation of ti-6Al-4V during high cycle fatigue at high R ratios. *Journal of the Mechanics and Physics of Solids, 129*, 61-82.

Birnbaum, A. J., Vikelic, S., & Yao, L. Y. (2010). Advances in laser-induced plastic deformation processes.

Blanc, C., & Aubert, I. (2019). *Mechanics - microstructure - corrosion coupling: Concepts, experiments, modeling and cases*. San Diego: ISTE Press Limited - Elsevier Incorporated.

Burlat, M., Julien, D., Lévesque, M., Bui-Quoc, T., & Bernard, M. (2008). Effect of local cold working on the fatigue life of 7475-T7351 aluminium alloy hole specimens. *Engineering Fracture Mechanics, 75*(8), 2042-2061.

Chakherlou, T. N., & Vogwell, J. (2003). The effect of cold expansion on improving the fatigue life of fastener holes. *Engineering Failure Analysis, 10*(1), 13-24.

Curtiss-Wright. (2018, August 16). Controlled Shot Peening Services from Curtiss-Wright. Retrieved from https://www.cwst.co.uk/services/controlled-shot-peening/

DOD. (2003). *Department of Defense Handbook: Metallic Materials and Elements for Aerospace Vehicle Structures*. Place of publication not identified, Washington D.C.: United States Department of Defense

Dowling, N. E. (2012). *Mechanical behavior of materials: Engineering methods for deformation, fracture, and fatigue*. Englewood Cliffs, N.J: Prentice Hall.

Drucker, D. C. (1951). *A more fundamental approach to plastic stress-strain relations* (pp. 487-491). Chicago, IL: U.S. National Congress of Applied Mechanics.

Findlay, S. J., & Harrison, N. D. (2002). Why aircraft fail. *Materials Today (Kidlington, England), 5*(11), 18-25.

Fu, Y., Ge, E., Su, H., Xu, J., & Li, R. (2015). Cold expansion technology of connection holes in aircraft structures: A review and prospect. *Chinese Journal of Aeronautics, 28*(4), 961-973.

Fung, Y. C. (1965). *Foundations of solid mechanics*. Englewood Cliffs, N.J: Prentice-Hall.

Gopalakrishna, H. D., Narasimha Murthy, H. N., Krishna, M., Vinod, M. S., & Suresh, A. V. (2010). Cold expansion of holes and resulting fatigue life enhancement and residual stresses in al 2024 T3 alloy – an experimental study. *Engineering Failure Analysis, 17*(2), 361-368.

Habiri, M. E., Benachour, M., & Benachour, N. (2018). Effect of cold expansion on improving of fatigue initiation life in aluminium alloy. *Frattura Ed Integritá Strutturale, 12*(46), 34-44.

Houghton, S. J. (2010). *Finite Analysis of the Cold Expansion of Aircraft Fastener Holes* (Rep. No. 295). Auckland, NZ: Defence Technology Agency.

Kang, J., Steven Johnson, W., & Clark, D. A. (2002). Three-dimensional finite element analysis of the cold expansion of fastener holes in two aluminum alloys. *Journal of Engineering Materials and Technology, 124*(2), 140-145.

Kim, S., & Kim, D. (2019). Interference-fit effect on improving bearing strength and fatigue life in a pin-loaded woven carbon fiber-reinforced plastic laminate. *Journal of Engineering Materials and Technology, 141*(2)

Leon, A. (1998). Benefits of split mandrel coldworking. *International Journal of Fatigue, 20*(1), 1-8.

Liu, J., Shao, X. J., Liu, Y. S., & Yue, Z. F. (2008). Effect of cold expansion on fatigue performance of open holes. *Materials Science & Engineering. A, Structural Materials: Properties, Microstructure and Processing, 477*(1), 271-276.

Liu, J., Xu, H. L., Zhai, H. B., & Yue, Z. F. (2010). Effect of detail design on fatigue performance of fastener hole. *Materials & Design, 31*(2), 976-980.

Liu, J., Yue, Z. F., & Liu, Y. S. (2007). Surface finish of open holes on fatigue life. *Theoretical and Applied Fracture Mechanics, 47*(1), 35-45.

Mahendra Babu, N. C., Jagadish, T., Ramachandra, K., & Sridhara, S. N. (2008). A simplified 3-D finite element simulation of cold expansion of a circular hole to capture through thickness variation of residual stresses. *Engineering Failure Analysis, 15*(4), 339-348.

Mello, A. W., Nicolas, A., Lebensohn, R. A., & Sangid, M. D. (2016). Effect of microstructure on strain localization in a 7050 aluminum alloy: Comparison of experiments and modeling for various textures. *Materials Science & Engineering. A, Structural Materials : Properties, Microstructure and Processing, 661*(C), 187-197.

Mostefa, B., Abdelkrim, A., Ali, B., & Mohamed, B. (2012). Effect of hardening induced by cold expansion on damage fatigue accumulation and life assessment of aluminum alloy 6082 T6. *Materials Research (São Carlos, São Paulo, Brazil), 15*(6), 981-985.

Nicolas, A., Mello, A. W., & Sangid, M. D. (2019). Relationships between microstructure and micromechanical stresses on local pitting during galvanic corrosion in AA7050. *Corrosion Science, 154*, 208-225.

Niu, M. C. (2011). *Airframe stress analysis and sizing* (3rd ed.). Adaso/Adastra Engineering Center.

Pasta, S. (2007). Fatigue crack propagation from a cold-worked hole. *Engineering Fracture Mechanics, 74*(9), 1525-1538.

Phillips, J. L. (1974). *Sleeve coldworking of fastener holes*. Ohio: Wright-Patterson Air Force Base.

Rice, R. C., Jackson, J. L., Bakuckas, J., & Thompson, S. (n.d.). *Metallic Materials Properties Development and Standardization (MMPDS)* (Rep. No. DOT/FAA/ AR-MMPDS-01). Washington D.C.: U.S. Department of Transportation - Federal Aviation Administration - Office of Aviation Research.

Sun, D., Lemoine, P., Keys, D., Doyle, P., Malinov, S., Zhao, Q., . . . Jin, Y. (2018). Hole-making processes and their impacts on the microstructure and fatigue response of aircraft alloys. *The International Journal of Advanced Manufacturing Technology, 94*(5-8), 1719-1726.

Wang, Y., Zhu, Y., Hou, S., Sun, H., & Zhou, Y. (2017). Investigation on fatigue performance of cold expansion holes of 6061-T6 aluminum alloy. *International Journal of Fatigue, 95*, 216-228.

Yasniy, P., Glado, S., & Iasnii, V. (2017). Lifetime of aircraft alloy plates with cold expanded holes. *International Journal of Fatigue, 104*, 112-119.

Zhang, X., & Wang, Z. (2003). Fatigue life improvement in fatigue-aged fastener holes using the cold expansion technique. *International Journal of Fatigue, 25*(9), 1249-1257.

APPENDIX A – Specimen and Material Information

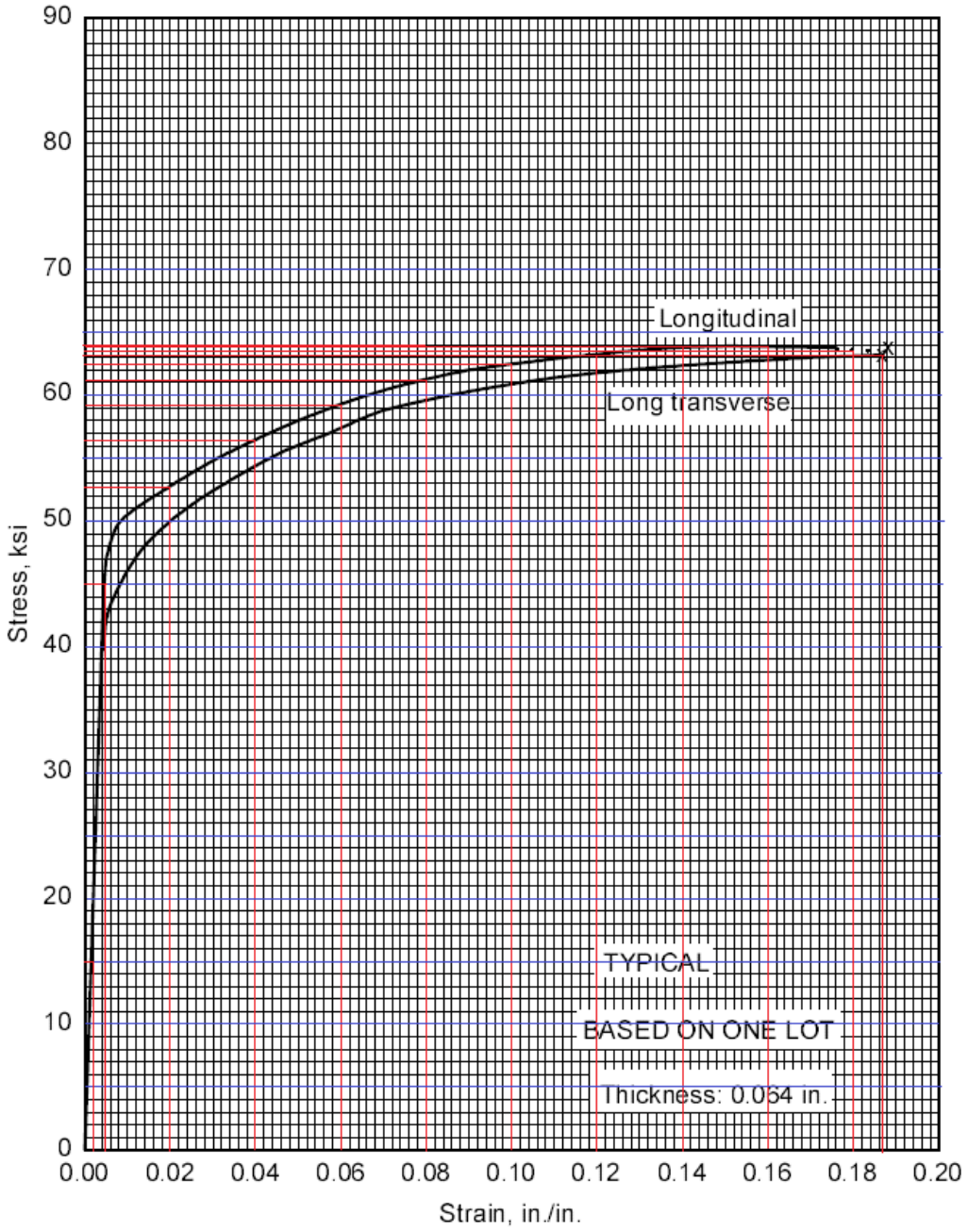

Figure A.1 Enlarged typical tensile stress v strain curve for Al 2024-T3 showing the mapping that was done to determine the Plasticity Modulus used for FEM simulations (Rice et al., 2016).

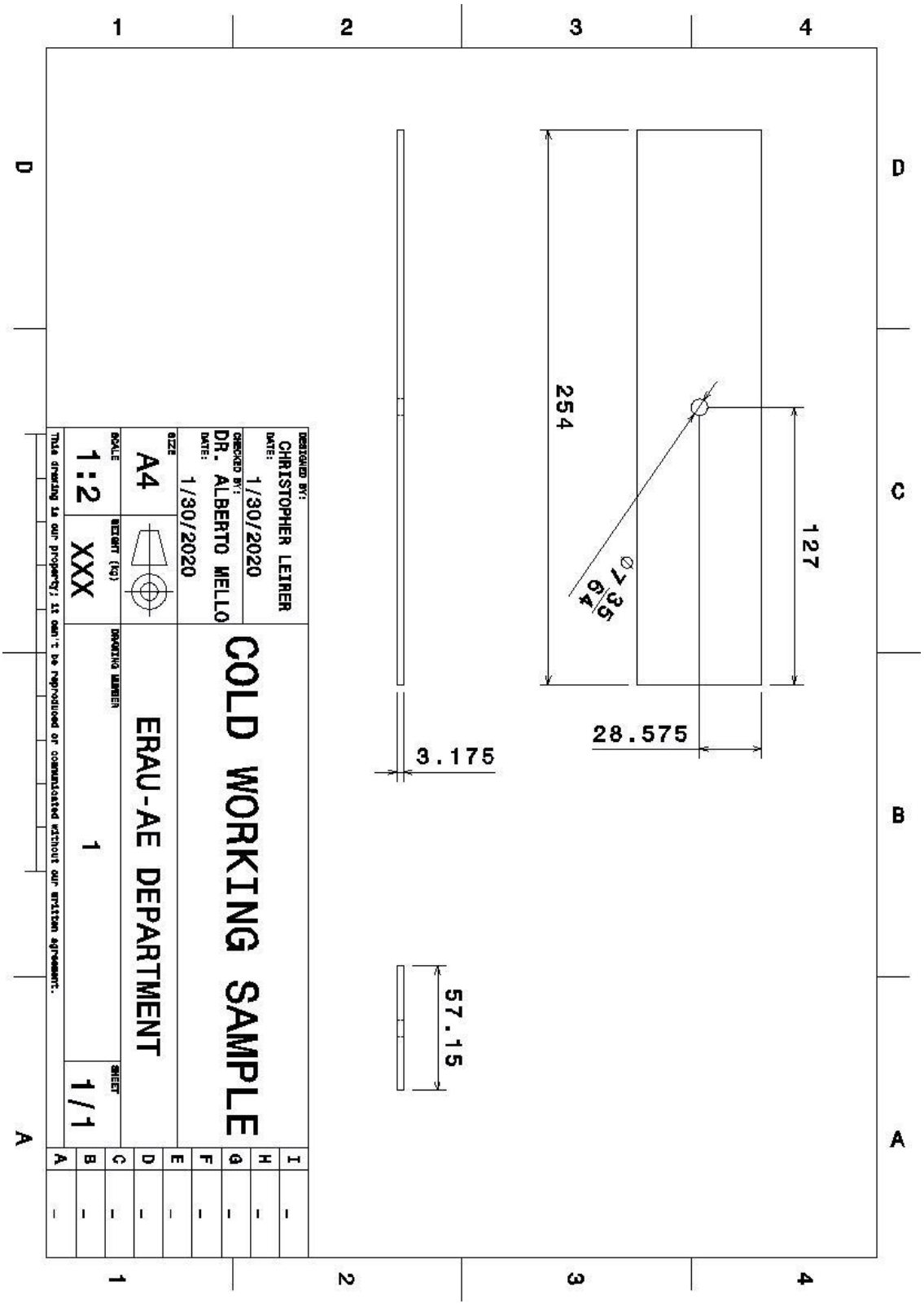

Figure A.2 Full scale engineering drawings of specimen dimensions provided to the Embry-Riddle Manufacturing Shop for specimen manufacturing.

APPENDIX B – FEM Contours of Cold Expansion

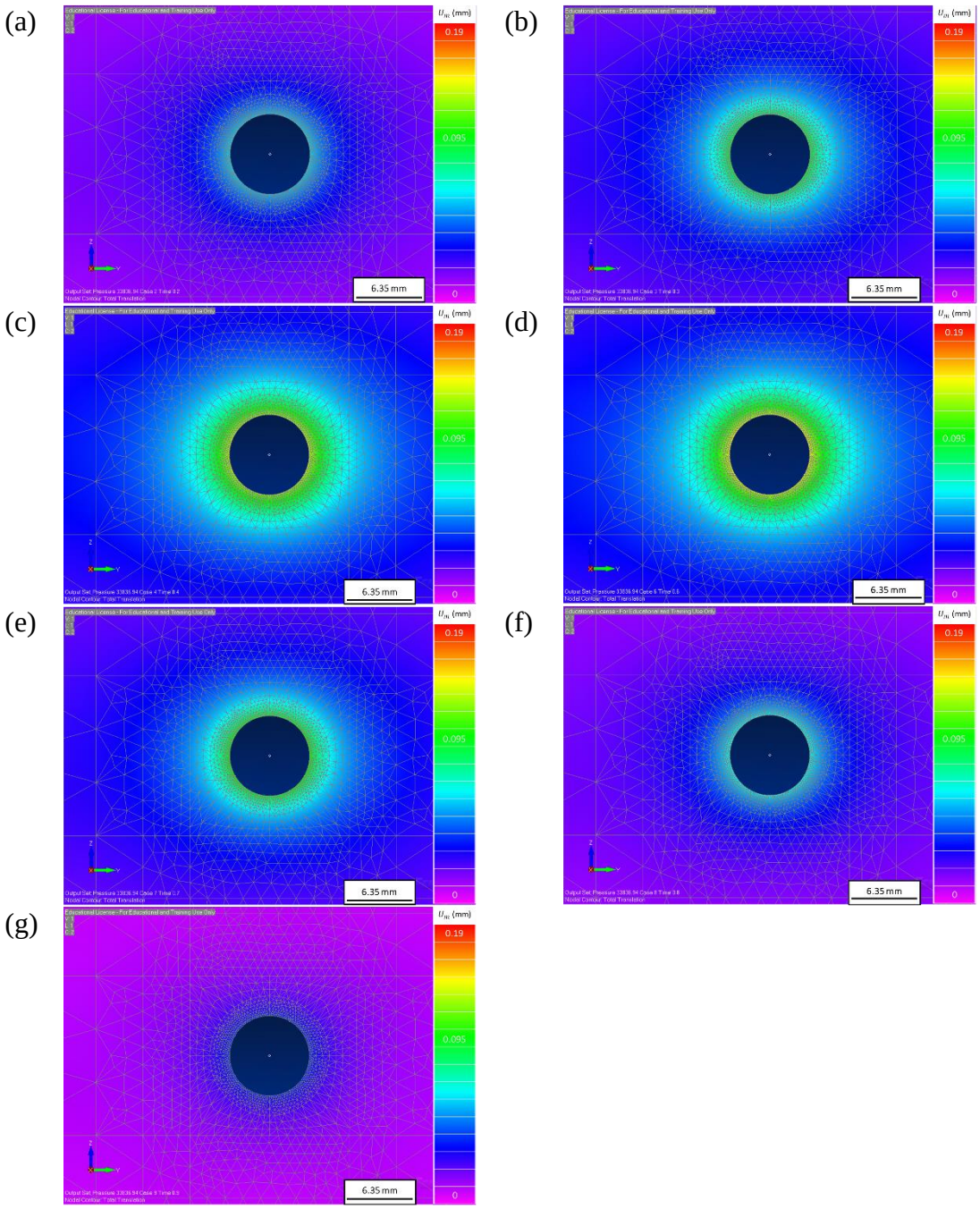

Figure B.1 Radial displacement development around hole during cold expansion process at corresponding times: (a) 0.2s (b) 0.3s (c) 0.4s (d) 0.6s (e) 0.7s (f) 0.8s (g) 0.9s.

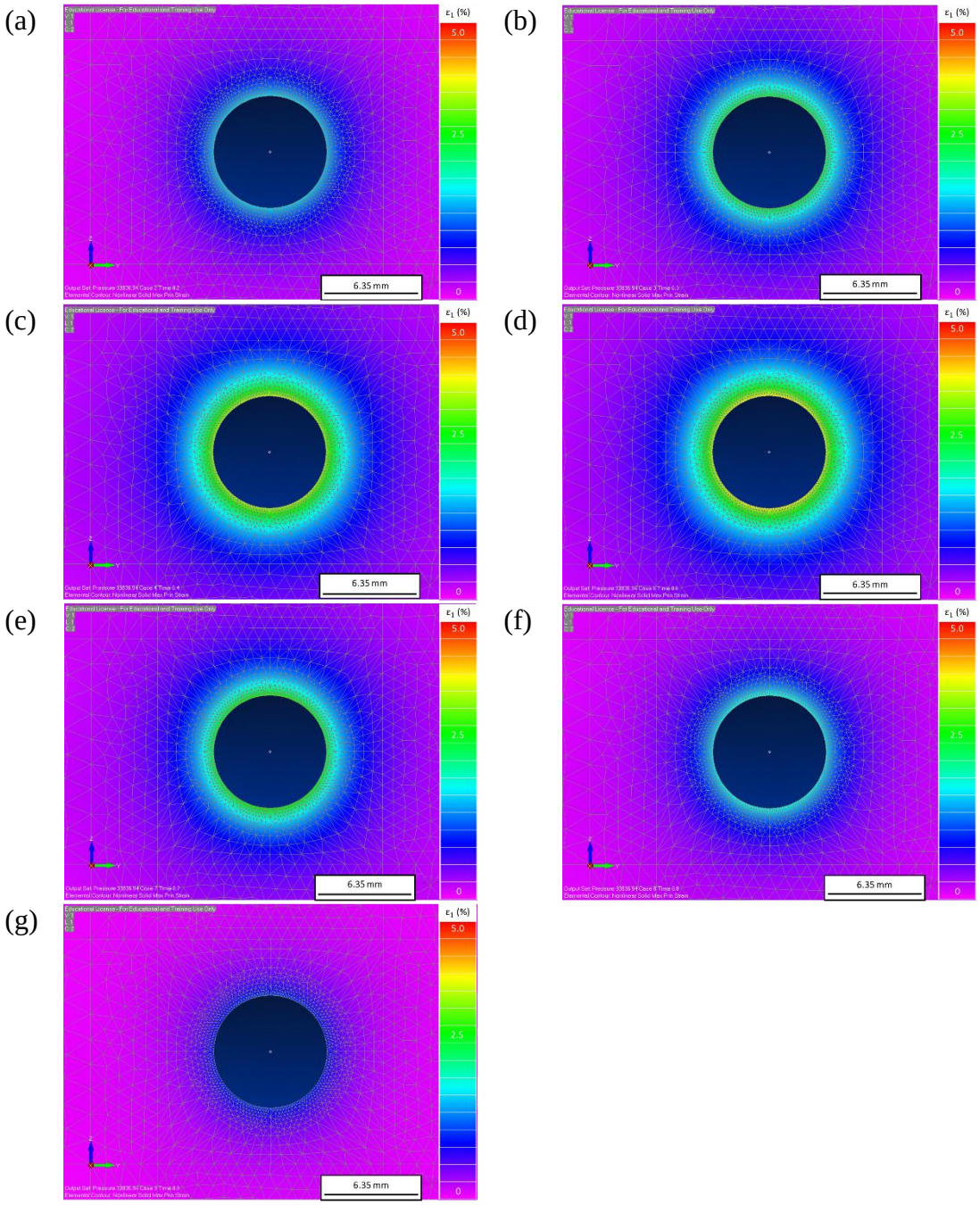

Figure B.2 Cold expansion degree development around hole during cold expansion process at corresponding times: (a) 0.2s (b) 0.3s (c) 0.4s (d) 0.6s (e) 0.7s (f) 0.8s (g) 0.9s.

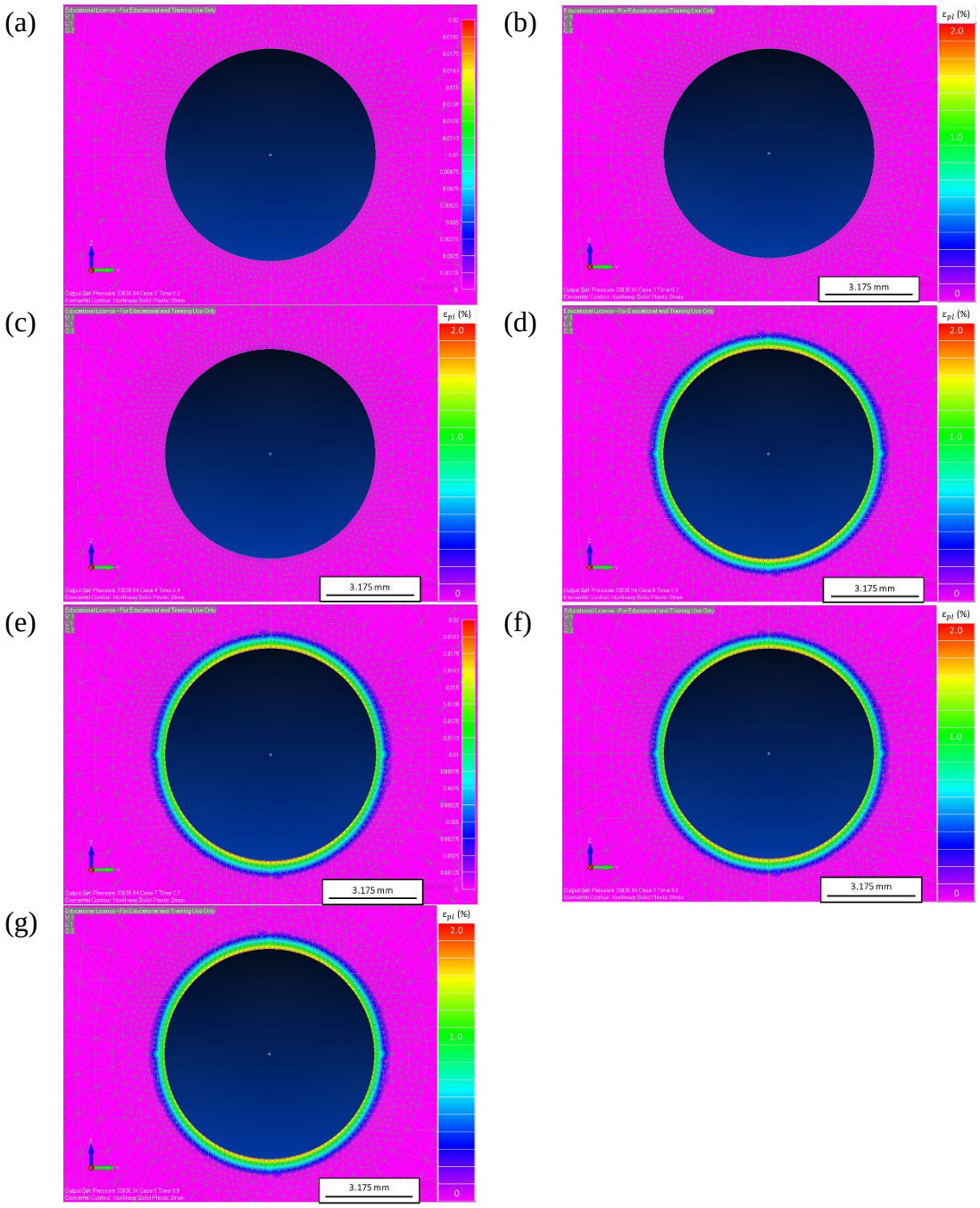

Figure B.3 Plastic strain development around hole during cold expansion process at corresponding times: (a) 0.2s (b) 0.3s (c) 0.4s (d) 0.6s (e) 0.7s (f) 0.8s (g) 0.9s.

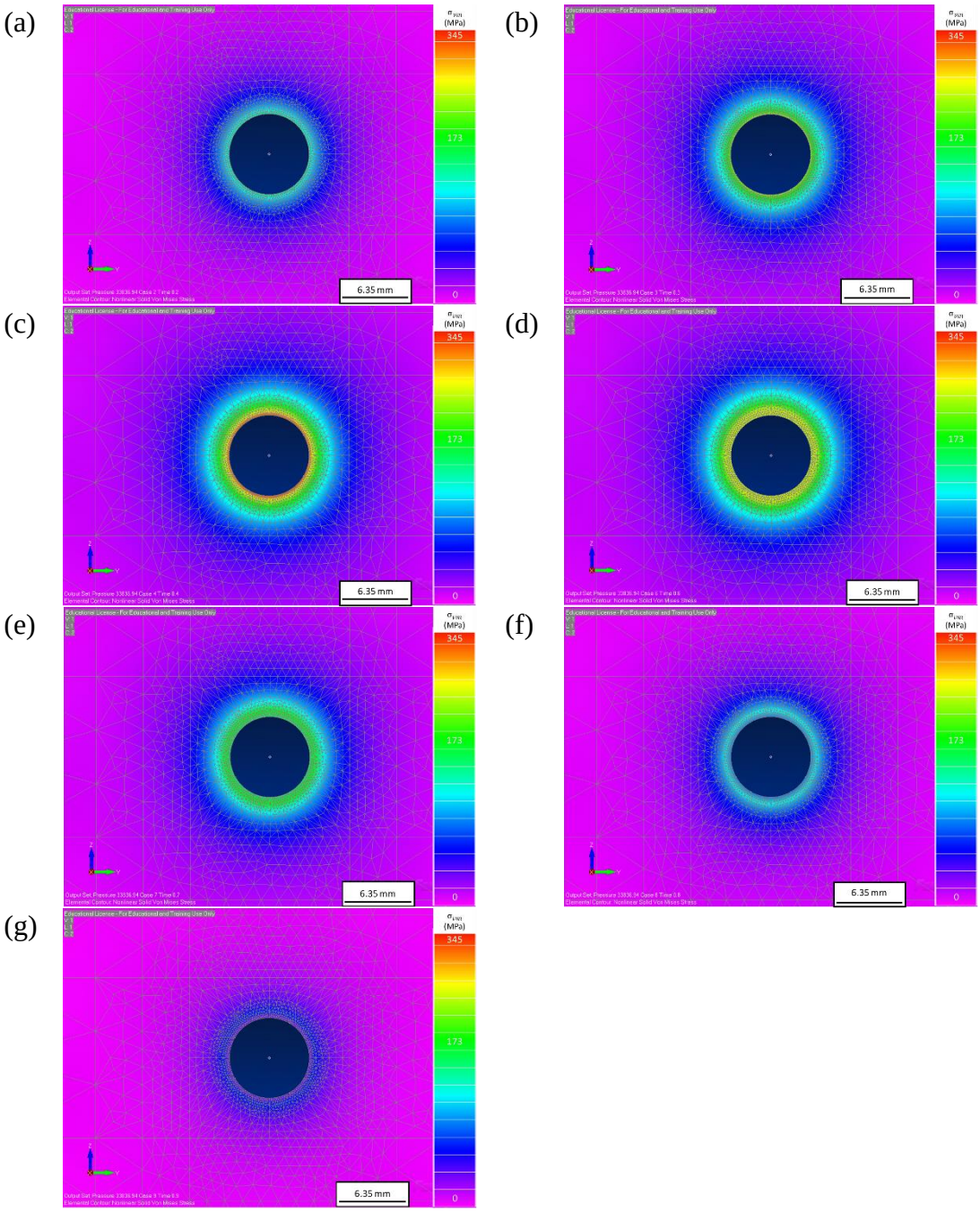

Figure B.4 Von Mises stress development around hole during cold expansion process at corresponding times: (a) 0.2s (b) 0.3s (c) 0.4s (d) 0.6s (e) 0.7s (f) 0.8s (g) 0.9s.

APPENDIX C – Speckle Analysis Tables

Table C.1

Initial speckle analysis using program suggested subset size for DIC calculations.

Sample	Distance m (ft.)	Layers	Subset Size	Std. Dev. (%)	Avg. % Strain
1	0.6096 (2)	3	45	0.0833	0.0793
2	0.3048 (1)	2	61	0.0662	0.0819
3	0.3048 (1)	1	53	0.0776	0.0742
4	0.6096 (2)	1	71	0.0531	0.0494
5	0.6096 (2)	2	63	0.0733	0.0688
6	0.6096 (2)	3	55	0.0614	0.0572
7	0.9144 (3)	1	113	0.0513	0.0304
8	0.9144 (3)	2	83	0.0478	0.0420
9	0.6096 (2)	1	77	0.0437	0.0446
10	0.6096 (2)	2	85	0.0425	0.0486
11	0.9144 (3)	2	109	0.0273	0.0272
12	0.9144 (3)	1	97	0.0306	0.0301
13	0.6096 (2)	1	83	0.0374	0.0357
14	0.6096 (2)	2	75	0.0576	0.0498
15	0.6096 (2)	1	93	0.0402	0.0393
16	0.9144 (3)	1	115	0.0271	0.0273
17	0.9144 (3)	2	95	0.0325	0.0348

Table C.2

Improved speckle analysis with manipulated subset size to improve DIC calculations.

Sample	Prev. Subset Size	Imp. Subset Size	Imp. Std. Dev.	Imp. Avg. % Strain
1	45	37	0.1004	0.0948
2	61	37	0.1553	0.1233
3	53	37	0.1190	0.1098
4	71	37	0.1200	0.1091
5	63	37	0.1386	0.1235
6	55	35	0.0976	0.0880
7	113	35	0.2567	0.2133
8	83	35	0.1486	0.1242
9	77	35	0.1176	0.1063
10	85	35	0.1272	0.1179
11	109	35	0.1273	0.1213
12	97	35	0.1205	0.1140
13	83	35	0.1073	0.1012
14	75	35	0.1474	0.1273
15	93	35	0.1372	0.1257
16	115	35	0.1311	0.1258
17	95	35	0.1181	0.1192